2018•2019

Faculteit Industriële ingenieurswetenschappen

master in de industriële wetenschappen: nucleaire technologie

Masterthesis

Dose verification in lung SBRT and implications with the clinical implementation of Acuros

PROMOTOR :

Prof. dr. Brigitte RENIERS

PROMOTOR :

Dhr. Koen TOURNEL

COPROMOTOR :

De heer Burak YALVAC

COPROMOTOR :

Mevr. Karin BAMPS

Lisa Dhamers

Scriptie ingediend tot het behalen van de graad van master in de industriële wetenschappen: nucleaire technologie, afstudeerrichting nucleaire technieken / medisch nucleaire technieken

Gezamenlijke opleiding UHasselt en KU Leuven

2018•2019

Faculteit Industriële ingenieurswetenschappen

master in de industriële wetenschappen: nucleaire technologie

Masterthesis

Dose verification in lung SBRT and implications with the clinical implementation of Acuros

PROMOTOR :
Prof. dr. Brigitte RENIERS

PROMOTOR :
Dhr. Koen TOURNEL

COPROMOTOR :
De heer Burak YALVAC

COPROMOTOR :
Mevr. Karin BAMPS

Lisa Dhamers

Scriptie ingediend tot het behalen van de graad van master in de industriële wetenschappen: nucleaire technologie, afstudeerrichting nucleaire technieken / medisch nucleaire technieken

UHASSELT KU LEUVEN

Foreword

Writing a thesis is not a self-evident matter. One works on it school year round, one wakes up with it and goes asleep with it. I consider this Master's thesis as the icing on the cake. After three years of education, of which two years of the bridging program and one Master's year, full of projects and exams, this Master's thesis represents the final piece of my study. All gained knowledge and schooling, scientifically and socially, I can now pack in this piece of work.

After a milestone like this, it's good to look ahead at what will come, but it's also necessary to look back at everything that has happened these last three years. All the friendships, the challenges, the 'hard' life of being a student and so on. It went by so quickly.

One does not write a thesis on its own. I had my prof. dr. Brigitte Reniers as internal promotor. She was always there to help me gain insights, to give me feedback, to help me get the software going again (after crashing over and over). She has always been open and honest to me and we laughed and joked a lot throughout the whole process. I would like to thank her for the explanation, the insights I gained and for sharing her experience on medical physics and beyond. Next to my professor, I would like to thank my internal co-promotor, project engineer Burak Yalvac, for his additional feedback on the writing and help during the practical study. Also, I could count on my external promotors, Koen Tournel and Karin Bamps. I would like to thank them for their guidance and for helping me during the crucial part of the phantom testing in the LOC, even far past their working hours. I thank Nathalie Reulens for the careful read out of the alanine pellets and Gabriel Fonseca for the conversion of the RTstructs to stl-files.

I dedicate my last paragraph to those who are truly close to me and supported me during this three year journey that often represented a challenging and bumpy road. In the first place, I would like to thank Willem Vancamelbeke. Thanks to him, I had the courage to pursue my dream and believe in myself. Next to Willem, I thank my parents for 25 years of guidance and for giving me the opportunity to, after my bachelor's degree Medical Imaging, get my Master's degree in Medical Nuclear Engineering. Finally, I cannot forget to thank my friends who were always there to support me, with their encouraging advice, positive attitude and contagious smiles.

Lisa Dhamers, May 2019

Table of contents

List of tables

List of figures

Abstract

The currently used standard in radiotherapy for dose calculation is AAA. Although more accurate and faster calculation engines are present, such as AcurosXB (Varian Medical Systems), the switch from AAA to AXB has not been made. Despite many previous studies, the implications on the dose are not ambiguously clear. This Master's thesis, in cooperation with Beldart, LOC Limburg and Maastro Clinic, focusses on the dose reporting and evaluation of lung SBRT.

The dose of PTV and OAR in SBRT plans was verified and evaluated for AAA and the two dose reporting methods of AXB: dose-to-water and dose-to-medium (AXB_W and AXB_M). Firstly, the dose differences of AAA, AXB_W and AXB_M were examined by recalculating 60 SBRT-plans. The absolute percentage difference for PTV and OAR were compared. Next, the dose (AAA), was verified with the Virtual Water Dose Verification Phantom with an adjustable hydrogel tumor. The dose maps of the TPS were evaluated and compared at the tumor center and at the lung-soft tissue transition with two radiochromic films. The dose at tumor center was verified with L-α-alanine.

Although the recalculations concluded an overestimation of AAA (5,6%) in comparison to AXB, the results in three phantom tests did not confirm this. The three individual phantom cases showed that dose differences are affected by several parameters, of which the surrounding tissue distribution is the most important. Further refining of the phantom is necessary, to minimize uncertainties and further evaluate the dose differences of the algorithms.

Abstract in Nederlands

De standaard in radiotherapie voor dosisberekening is AAA. Hoewel er accuratere en snellere algoritmes op de markt zijn, zoals AcurosXB (Varian Medical Systems), is het moeilijk om over te stappen van AAA naar AXB. Ondanks reeds vele studies, zijn de implicaties op de dosis van een switch naar Acuros niet eenduidig. Deze masterproef, in samenwerking met Bel*d*art, LOC Limburg en Maastro Clinic, spitst zich toe op de dosisrapportering en -evaluatie bij long SBRT.

De dosis van PTV en OAR bij SBRT-plannen werd geëvalueerd voor AAA en de rapporteringsmethodes van AXB: dose-to-water en dose-to-medium. Eerst werden de dosisverschillen van AAA, AXB_W en AXB_M onderzocht door herberekening van 60 SBRT-plannen. De absolute procentuele verschillen voor PTV en OAR werden vergeleken. Ook werd de dosis (AAA), geverifieerd en geëvalueerd met het Virtual Water Dose Verification Phantom met aanpasbare hydrogel tumor. De dosismappen van het TPS werden geëvalueerd en vergeleken in het centrum van de tumor en op de overgang long-zacht weefsel door 2 EBT3 films. De dosis in het centrum van de tumor werd geverifieerd met L-α-alanine.

Ondanks dat de herberekeningen een overschatting van AAA (5,6%) tegenover Acuros rapporteerden, bevestigden de individuele fantoomtesten dit niet. Zij toonden aan dat de dosis beïnvloed wordt door meerdere parameters, waarbij de weefselsamenstelling de meest doorslaggevende is. Verdere verfijning van het fantoom is nodig, om onzekerheden te minimaliseren en de dosisverschillen tussen de algoritmes verder te onderzoeken.

1. Introduction

This Master's thesis focusses on the dose evaluation of lung SBRT. Although faster and more accurate dose calculation algorithms are on the market, the Anisotropic Analytical Algorithm (AAA) remains the current standard in the clinic. Despite many previous studies of the dose differences between AAA and Acuros, a switch from AAA to AcurosXB (Varian Medical Systems, Palo Alto, CA, USA) remains absent. Are there reasons to believe that a switch to Acuros is not a good idea?

In this thesis, the dose effects of the current standard dose calculation engine, Anisotropic Analytical Algorithm (AAA), are compared to the dose effects of Acuros. This comparison was done using different techniques, which will be explained extensively in the literature study.

The dose differences will be evaluated for the two different dose reporting methods of Acuros, dose-to-water (AXB_W) and dose-to-medium (AXB_M). A general overview was created by recalculating 60 existing lung SBRT-plans for Acuros (AXB_W and AXB_M) to compare the dose of the delineated volumes. Next, a dose verification phantom was developed to verify the AAA dose to the film. Two dosimeters, L-α-alanine and EBT3 radiochromic films, measured the dose in the phantom. By using two radiochromic films, one at the lung tissue-soft tissue boundary above the tumor, and one at the center of the tumor and L-α-alanine at the center of the tumor, the dose distribution of the tumor and surrounding tissue could be evaluated.

The phantom was irradiated for three separate tests and afterwards, the dose for the different algorithms was evaluated and compared using a slab phantom with adjustable hydrogel tumor. Several materials were tested to explore lung tissue and tumor tissue equivalence. The entire procedure and the preceding material tests are described in the section 'Method and Materials'.

After testing, first of all, the outcome of the tissue equivalence tests is mentioned in 'Results'. In the second paragraph, the results of the phantom tests are displayed: the calibration curve, used for the film dosimetry; the alanine/EPR dosimetry used in the study; the recalculations of the 60 SBRT plans. Lastly, the dose maps and horizontal profiles of the three phantom tests are compared for the different algorithms and the EBT3 films using graphs and gamma dose maps.

This thesis is a first step in the process to develop a suitable phantom for an End-To-End test as part of a new lung SBRT external dosimetry audit procedure for BEL*d*ART and at the same time this study tries to find a clear answer or explanation if a AAA-Acuros switch is possible or not.

2. Literature

2.1. SBRT

Lung cancer is one of the most common types of cancer worldwide, responsible for the highest number of cancer deaths [1].
20-25% of the patients who are diagnosed at an early stage undergo surgical abscission. However, 20-30% of all lung cancer patients cannot be operated or is unwilling to undergo surgery. The primary alternative treatment is external beam radiotherapy (EBRT). In conventional external beam radiotherapy, patients are treated with a total radiation dose of 60-70 Gy, in 30-35 daily fractions of 1,8-2,0 Gy per day. Yet, for patients with stage I and II lung tumors, radiotherapy treatment shows remarkably inferior results compared to surgery, with local recurrence rates up to 70% [1],[2].
Research on the effects (local tumor control and toxicity) of hypofractionation in radiation treatment of small targets in dose-escalation studies, has led to a new form of external beam radiotherapy: Stereotactic Body Radiotherapy (SBRT) or Stereotactic Ablative Radiotherapy (SABR). This method involves very precise delivery of one or more high dose fractions (>10Gy per fraction), typically 3-5 fractions, to the tumor volume which yields excellent local control [3],[4].
This stereotaxy technique was developed at the Karolinska institute in the early 1990s and initially only applied in cranial radiosurgery. Afterwards SBRT also targeted patients with a deteriorated lung capacity (inoperable stage I lung cancer). Due to its success, SBRT also acquired approval in operable patients. Thanks to technological improvements in motion management and image guidance the patient range for this technique could be extended. Because of higher accuracy in radiotherapy delivery treatment and an increasing amount of challenging patient cases, more patients were proven to be suitable for an SBRT treatment [5].
Since then, along with the developments in radiotherapy technology and techniques (e.g. 4DCT simulation and image guided radiotherapy (IGRT)), this has led to the increase of SBRT in a number of clinical situations, especially in lung SBRT for both early stage lung cancer and lung metastases [1],[6],[7].

2.2. EBRT vs. SBRT

The radiobiological principles and effects for conventional EBRT can be translated in several dose response models, such as the linear-quadratic (LQ) model. This model takes into account the effects of cell death caused by DNA breaks. However, SBRT with extreme hypofractionation (>10 Gy/fraction), not only kills tumor cells by DNA strand breaks. SBRT also causes significant direct damage in tumor vasculatures as well as microvascular dysfunction and secondary tumor cell death. Such fulminant vascular damage results in endothelial apoptosis and probably indirectly causes an immune response against the tumor due to the use of high radiation doses per fraction. Hereby a rapid dose fall-off is necessary, with maximizing of the dose to the tumor volume (up to 140 % of the mean dose) while keeping dose to normal structures minimal [1], [4], [8], [9], [10].
Hypofractionation in EBRT has several benefits: firstly, the restrained repopulation of neoplastic cells; secondly, a better economical outcome; and finally, more convenience for patients, in comparison to classical fractionation [11].

All these additional effects of SBRT have not been accounted for in traditional tumor response models, such as LQ model. Recent clinical results have shown that the LQ model likely underrates the tumor control by SBRT. Hence, the use of this model is limited for high doses (>10 Gy) as in SBRT [9], [12], [13].
Setting dose–volume constraints or designing a biological model for the optimization of SBRT is especially venturous when the used parameters are deduced from a classical fractionation scheme. The AAPM TG 166 recommends to only adjust dose limits that lead the dose of OAR in a dose range that is known to be clinically safe, since there is no scientific research done on a possible biological model for SBRT optimization yet [13], [14], [15].

2.2.1. Technical aspects of an SBRT treatment

Before a patient can be treated, several steps have to be considered to provide a precise and personal treatment plan. After cancer diagnosis, in this case stage I or II lung cancer, a treatment method needs to be chosen. Depending on the tumor size, stage, position and tumor type EBRT, SBRT, surgery, chemotherapy or a combination of these treatment methods will be prescribed. All these different factors are taken into account to ensure the greatest survival rate.
In the case of SBRT treatment, firstly the target needs to be localized with CT imaging, secondly all treatment margins need to be defined. Thirdly, dose planning and calculation is layed out following the dose prescription. Lastly, the tumor localization is ensured using in-room image guidance during treatment. If the tumor has changed too much between fractions, a new treatment plan needs to be set up.
The handling of all these steps will decide the inter- and intrafractional accuracy of the dose delivery, and should be handled with suitable treatment margins [5].

SBRT also demands for high quality imaging for treatment planning, with superior visualisation of the target that permits precise tumor delineation. Therefore, four dimensional CT (4DCT), which includes the patients' respiratory cycle, is used, with or without externally measured respiratory signal. In order to locate and delineate the tumor with high precision, high spatial resolution imaging is necessary. For CT images used for SBRT, a slice thickness of ≤ 2 mm is preferred.
Tumors situated in the lung, can move in a complex or irregular pattern during respiration. Subsequently, respiratory motion can deteriorate the image quality in all imaging modalities, regardless of the use of respiratory trackers or not. This needs to be taken into account during imaging and treatment [5].

Imaging, just before treatment ensures a correct delivery of the treatment plan to the tumor volume and surrounding OAR. With the help of electronic portal imaging devices (EPID), image guided ratiotherapy (IGRT) became more widely available, facilitating 2D MV and kV imaging of various treatment fields. To reduce inter- and intrafraction uncertainties, monitoring is preferred since this might disclose undetected shifts in the patient's anatomy.
Various approaches were used throughout the implementation of lung SBRT to control the respiratory movement: breath hold, abdominal compression, gating and tracking. However, the efficiency of certain strategies have been questioned in their ability to reduce uncertainties, and it is important to realize that none of the methods mentioned above entirely cancels out breathing-related uncertainties. In addition, some strategies may only be possible in patients with relatively good breathing performance and who are willing to do so. These techniques demand active patient cooperation (breath hold), can create discomfort (abdominal compression) or extend the treatment time (gating) [5].

Intra-fraction CBCT images through reconstruction of the 2D kV CBCT images during treatment, makes verification of the tumor position and movement of the tumor during free-breathing possible, while the treatment beam is on. Residual intra-fractional uncertainties of the tumor position can lead to systematic and random errors within 2 mm, and need to be taken into account when determining the treatment margins [5].

The gross tumor volume (GTV) takes into account the macroscopic visible tumor volume. Often a clinical target volume (CTV) applies a small margin around the GTV to include microscopic spread of the tumor, which is not yet visible on imaging. To account for all set-up uncertainties, internal organ motion and geometrical errors, a margin for the planning target volume (PTV) is added.
Despite this logical approach, the uncertainties on the treatment margins of a tumor, that is subject to breathing or bowel movement, should not be added linearly. This approach leads to an unnecessarily large margin anterior-posterior and left-right direction and a margin not large enough in the caudocranial direction.
An alternative is the fusion of the delineated GTV volumes in all breathing phases, which practically involves delineating the GTV on the maximum intensity projection (MIP) images and fusion of GTVs from all respiratory phases of a 4DCT. Another approach on motion management is the use of midventilation, in which the time-averaged tumor position is subject to margin probabilities [5], [14].

2.2.2. Dose calculation algorithms

In external beam radiotherapy in general, heterogeneities introduced by different materials such as lung, bone, air and non-biological implants, i.e. materials with either very high or very low HU-values, affect the absorbed dose in the patient, especially in the presence of small or irregular fields. Therefore, there is a need for more accurate (and complex) dose calculation algorithms used by the Treatment Planning System (TPS) [16].
In 2010, Varian Medical Systems released Acuros XB (Varian Medical Systems, Palo Alto, CA, USA), a new and advanced dose calculation algorithm in the Eclipse Treatment Planning System that answers two strategic needs of modern radiotherapy treatment planning: a reduced dose calculation time and improved dose calculation accuracy [17], [18].

2.3. Evolution of dose calculation algorithms

Throughout the history of dose distribution algorithms, three generations of algorithms have been used. Type A algorithms such as pencil beam handle heterogeneities by solely scaling the beam density in longitudinal direction and do not account for the changes in electron transport. They were quickly replaced by type B algorithms. This kernel-based model, containing a nominal model for lateral scatter, estimates the dose delivery by calculating the density of the surrounding tissues through superposition-convolution [19]. The Anisotropic Analytical Algorithm (AAA) is a type B algorithm. The beam model in AAA is based on three separate convolution models. Firstly, a separate convolution of the bremsstrahlung photons is done. Brehmsstrahlung photons are the photons created through interaction of the initial electron beam and the target. Secondly, a convolution model for photon scattering in the primary collimators, the jaws and the flattening filter is added. A third convolution kernel takes into account the dose cause by electrons created in the linac head and in air, mostly through Compton interaction. The final dose is based on the convolution and calculation of the individual beamlets of the above mentioned three sources. AAA includes tissue heterogeneities firstly, by using radiological scaling of the dose deposition functions. Next, through radiological scaling, a scaling based on the

electron density in each voxel of the photon scatter kernels is done, and this in all four lateral directions [16], [20].
As opposed to commonly used type B-algorithms which are kernel-based, or Monte Carlo methods which use a statistical approach, the Acuros algorithm is based on direct numerical solving of the Linear Boltzmann Transport Equation (LBTE). The LBTE describes the behavior of radiation particles as they travel through and interact with matter [20], [17].
In explicit LBTE solution methods, the errors are mainly systematic, and emanate from discretization of the solution parameters in space, angle, and energy. A trade-off between speed and accuracy exists for either explicit and implicit LBTE method. The actual incentive of the development of explicit LBTE solution methods in general was to shorten the calculation time and have a rapid alternative to Monte Carlo simulations.
When compared to the current gold standard of Monte Carlo simulations, Acuros has proven an equivalent accuracy for the energy range 4-25 MeV produced by clinical linear accelerators and for a wide scope of physical materials and densities, from air to steel. Secondly, calculation times are only slightly affected by the number of fields in a plan. This means that a volumetric modulated arc (VMAT) plan is calculated almost as fast as a single field. The calculation time for a single field or few fields can be slower with Acuros than with Anisotropic Analytical Algorithm (AAA) but as the number of fields increases, Acuros becomes much faster than AAA [14], [17].
Both AAA (type B) and Acuros are available in the Eclipse TPS. Since the Acuros algorithm uses the same treatment machine head model as AAA, the AAA beam data can be imported in the Acuros beam model and only requires reconfiguration before it is ready to be used for dose calculations. This approach makes it very accessible and exact to compare these different methods with the exact same treatment plan [17].
With the clinical introduction of Monte Carlo or LBTE-algorithms a new challenge in dosimetry was created: in reference dosimetry and calibration, absorbed dose is based on measurements in water phantoms and thus defined in terms of dose-to-water. Because of this, treatment planning systems handle different voxel densities as water with variable electron density [21].
The first part of this work is to compare actual clinical plans of patients. Plans were created with the AAA algorithm and then copied and recalculated with the Acuros algorithm, for dose-to-water (AXB_W) and dose-to-medium (AXB_M), using the Varian Eclipse TPS. The second part of this Master's thesis is verifying the irradiated dose (AAA) to the calculated dose map in AAA as well as the recalculated dose maps in Acuros for AXB_W and AXB_M with a lung phantom with a hydrogel tumor.

2.4. AXB_W versus AXB_M

Acuros contains two different dose reporting methods: dose-to-water and dose-to-medium. To obtain the dose in each voxel, the fluence-to-dose response of the electrons is applied. This fluence-to dose response is dependent of the related energy of the electrons. For AXB_M, the material properties of the desired voxel are used to acquire the macroscopic energy deposition cross-section and atomic density. For AXB_W, the energy deposition cross-sections of the corresponding media are used [14], [16], [18].

2.4.1. Delivery techniques in lung SBRT

The implementation of volumetric modulated arc therapy (VMAT), especially in combination with flattening filter free (FFF) beams at dose rates of 2400 MU per minute, makes lung SBRT treatment delivery much faster and more convenient than the combination of multiple static beams.
Delivery of lung SBRT plans using FFF VMAT therapy has been proven to be beneficial with tolerable toxicity rates, although SBRT plans are also delivered with linacs with a flattening filter (FF) [5].
Reggiori [22] states that there were no statistically significant differences found between FFF and FF results. With regard to PTV coverage, targets of intermediate size favor FFF beams, while FF proved to be more suitable for smaller (<100 cm^3) and larger (>300 cm^3) targets. Also, plans treated with FFF beams have shown to spare more healthy tissue, in 85 % of the cases. Plans that were optimized without FFF beams seemed to have a higher average MU/Gy than plans delivered with FF beams. However, a notable and significant difference was observed in the beam-on time (BOT) between the plans delivered with and without FF beams. Plans delivered with FFF beams had a BOT that was four times lower than the BOT in plans delivered with FF beams [22].

2.5. Dose verification in a phantom

Currently, the most common approach to intensity modulated radiotherapy (IMRT) delivery QA comprises delivering the IMRT plan to a phantom and afterwards comparing the 2D dose distribution calculated by the TPS with the measured dose distribution on the radiochromic films. By using alanine, the absolute dose can be measured precisely and the calibration curve of the radiochromic EBT3 films can be adjusted to the right dose [23].

2.5.1. Properties of 3D printed materials

3D printing, or rapid prototyping, makes it possible to build a model or design by using simple computer-generated instructions in a remarkable short period of time, days to even hours. In the radiotherapy society, 3D printing has raised a great interest because of its ability to construct custom made phantom materials fast and often very economical when compared to the price of commercial phantoms. Models can be printed with a high level of detail and precision. Today, a broad range of 3D printing raw materials, from plastic to resins, is available. The structural stability of 3D printed models is similar to that of commercial phantom materials [24].
Currently, various 3D printing techniques are used, of which Fused Deposition Modeling (FDM) is one of the most common. In FDM, a thermoplastic is heated until it liquifies and afterwards ejected onto a thin FDM surface to construct the separate layers of a model, one by one. One of the thermoplastics that is used typically is Polylactic Acid (PLA). In FDM, the filament is ejected in a grid or typical honeycomb structure, which makes small air gaps on a sub-millimeter scale unavoidable, even in prints with the highest possible density. Although this used to be implied as a weakness of the FDM printing process, the air gaps in these parts do not influence their level of utility for radiation dosimetry, it is just because of these air gaps that it is possible to simulate low density materials such as lung tissue [24].

2.5.2. EBT film dosimetry

In radiotherapy, accurately determining the dose and precisely delivering the dose to the target is directly correlated with improved treatment results. This implies a higher tumor control and lower post radiation therapy complications. Over time, film dosimetry has become a powerful tool for dose evaluation and verification in radiation therapy and QA. There are important features as well as restrictions to radiochromic films, that have their influence on the performance of film dosimetry [25].

EBT3 Film properties

Radiochromic film was confirmed to be a precise quantitative 2D dosimeter with good spatial resolution for applications in EBRT, including IMRT quality assurance (QA), commissioning of treatment procedures and verification of the TPS [26].

Measuring dose with radiochromic EBT3 film (GAFCHROMIC™, International Specialty Products, Ashland, Covington, USA) facilitates not only high spatial resolution, but also weak energy dependence in a wide range of beam qualities in radiotherapy and finally near tissue equivalence in small radiation fields with high dose gradients such as in SBRT. Depending on the thickness of the sensitive layer, the number of sensitive layers and the composition of the sensitive layer, the sensitivity and uniformity will improve [25].

EBT3 films are made by coating a single layer, with a thickness of 27 μm. This active layer involves the active component, marker dye, stabilizers and other additives, which induces the low-energy dependence of the film. The marker dye diminishes the UV light sensitivity and used with a red green blue (RGB) film scanner, enables all the benefits of multichannel dosimetry. This active layer is covered by two identical transparent polyester substrates, each 120 μm thick, which makes the product more robust and waterproof. In comparison to the previous EBT radiochromic films (EBT2), the active layer composition and response remained unchanged, although some improvements were made: the symmetric structure avoids the potential errors in optical density measurements; a special surface treatment with microscopic silica particles prevents Newton's Rings formation [23], [26], [27].

Radiochromic films experience a color change directly after irradiation and do not need any chemical processing. They can be read out with a normal flatbed document scanner. This induces certain uncertainties which should be taken into account when determining the dose distribution of the film [25].

Sorriaux states that the red channel is the most sensitive for EBT3 for the dose up to 12 Gy for photon beams and the green channel has the highest sensitivity to the dose in a range of 12- 20 Gy and should be favored. Evaluation of the green channel instead of the red channel was suggested for doses of up to 4000 cGy, which is also confirmed in another study, performed by Khachonkham, where green channel evaluation seemed much more advantageous for doses higher than 500 cGy [23], [28], [29].

Radiochromic film dosimetry system – Clinical evaluation

By following a certain protocol, a film dosimetry system can provide an absolute dose by performing a measurement. However, to transform the film response (change in optical density) into absolute dose, a calibration curve needs to be set up. This calibration curve is established for a certain radiochromic film dosimetry system, with a particular film model (more specifically the film batch) and particular protocol, under reference conditions with a reference radiation beam quality. A dosimetry system that meets these requirements is acknowledged as a reference dosimetry system [25].

One Scan Dosimetry protocol

Lewis et al. [26] developed a one scan dosimetry protocol which gives the ability to produce only one single and general calibration curve for each lot of EBT3 films, applicable under a prescribed set of conditions. This new protocol combines calibration and measurement in a single scan to allow dose measurements of the application film and reference film, exposed at different times. In addition, the protocol focusses on the accuracy and integrity of the measurement by eliminating uncertainties due to the environment (humidity and temperature) and interscan variations [26].

The one scan dosimetry protocol of Lewis et al. [26] is not radically different from customary protocols such as TG-55 [30], but it simplifies film calibration in two ways. Firstly, by minimizing the number of dose points in the calibration curve and secondly, by combining digitization of the application film with the digitization of two reference films.

Reference to recommended calibration procedures claims that at least 15 dose points (and up to 45 points) are required [31]. The one scan dosimetry demands not only substantially less dose points, it allows all the calibration films to be scanned at once, because a rational function is used for the data points of the calibration instead of a polynomial function. This eliminates issues from interscan variations and reduces the overhead in workload and materials.

Polynomial functions are generally used to fit dose-response data. For dose-response data up to 4-5 Gy, this function is satisfactory. But, due to the increasingly nonlinear response of the radiochromic film with increasing dose range, the polynomial function does not fit for broad dose ranges. The function tends to oscillate between the data points at higher doses.

Figure 1 depicts the oscillating of the polynomial function at higher doses for the red channel in EBT3 film. However, the oscillating behavior does not resemble the actual behavior of radiochromic film. Radiochromic films darken in a monotonic fashion with increasing dose as the response asymptotes to a constant value. A solution to avoid this faulty polynomial fitting is to add more calibration points at higher doses, but this will again increase the workload and materials.

Hence, Lewis et al. [26] proposed the following fitting function:

$$X(D) = a + \frac{b}{D-c} \qquad (1, [26])$$

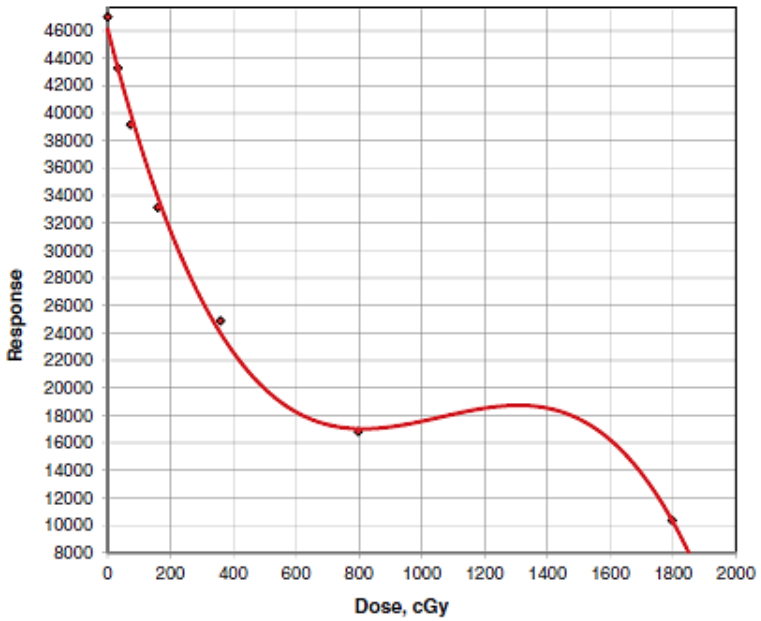

Figure 1: Dose-response data fit to polynomial function (3rd order) [25, p2]

This simple rational function, wherein X(D) depicts the response at dose D, and a, b and c are constants, has similar qualitative behavior as film. At high doses, X(D) converges to the value of a.
Figure 2 illustrates the fit of the rational function for the same data used to fit the polynomial function in Figure 1.

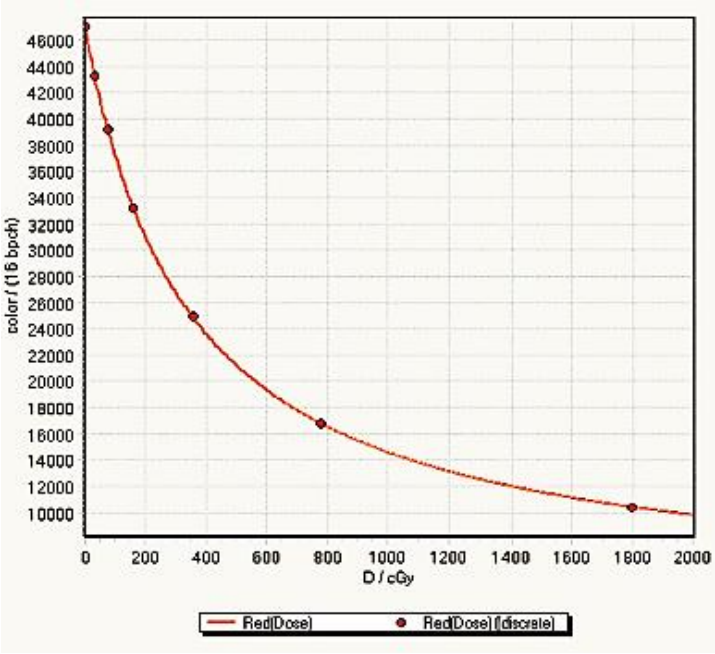

Figure 2: Dose-response data fit to rational function $X(D) = a + \frac{b}{D-c}$ [25, p3].

The rational function is a steady function, without oscillations and can be obtained with only three data points. Using a few more data points (4 or 5) in geometric progression can improve the fit and provides adequate agreement to assess dose measurements of IMRT plans.

The one scan dosimetry not only decreases the number of data points needed for calibration, it also combines the digitization of the application film with the digitization of two calibration films from the same production lot as the application film i.e. all three films are scanned simultaneously in one and the same scan. The two calibration films consist of one film exposed to a known dose and a second unexposed film. In addition, the exposed film needs to receive a dose 20% higher than the highest dose expected on the application film. By following this procedure, effects of scanner variations (between calibration and measurement) and temperature differences are eliminated [26].

Evaluation of uncertainties in EBT3 Film using triple-channel method and FilmQA Pro Software

Since radiochromic film has become an important tool to verify dose distribution for IMRT and QA procedures, it is important to understand the uncertainties that are involved when using radiochromic films [32]. The uncertainties associated with the intrinsic characteristics of the radiochromic film and the total uncertainty of the dosimetry system must be understood really well.

Many sources of uncertainties are involved in film dosimetry. Bouchard et al. arranged the different sources of uncertainties into five categories: film manufacturing (film homogeneity), film manipulation (storage, cutting), film irradiation (phantom, setup), film digitalization (flatbed scanner), and film response characterization with absorbed dose (fitting calibration function) [31], [33]. This is certainly the case with single channel dosimetry, where only one channel, mostly the red channel, is used to read the dose. However, by using all three color channels of the film and not only the red channel, many uncertainties can be eliminated or significantly reduced. The triple-channel evaluation is made possible with the FilmQA Pro Software (Ashland Inc, Covington, USA). It is a quantitative analysis tool, designed for film scanning, pixel value extraction, pixel value conversion to dose, and comprehensive dose analysis. The ability to use pixel values from all color channels together in dose map construction, providing corrected red, green and blue dose maps for further analysis [33]. The triple-channel method has proven to effectively separate nondose-dependent abnormalities from radiochromic film images. Also, disturbances caused by nonhomogeneities of the radiochromic film and artifacts caused by the scanner are removed which improves the integrity of the dose information. Furthermore, multichannel dosimetry permits compensation for thickness nonuniformities in the film, increases the signal to noise level, diminishes the lateral dose-dependency of flatbed scanners effect of the calculated dose map and finally extends the evaluable dose range from 10 cGy to 100 Gy [27].

A total uncertainty of minimum 3 % in single channel dosimetry can be reduced to less than 1 % in triple-channel dosimetry [34].

2.5.3. Alanine and EPR dosimetry

Small field dosimetry requires a dosimeter that is first of all, small, secondly does not cause disturbances or discontinuities in the volume in which the system is present and above all measures the dose accurately.

Alanine Electron Paramagnetic Resonance dosimetry (EPR) is an old yet still state-of-the-art dosimetry technique, not only because of its sensitivity improvements over the years but also because alanine fulfills several clinical applications. Besides the water-equivalent composition of alanine, its response is reasonably independent of the energy range (above 100 keV) and is dose rate independent in radiotherapy applications [35], [36].

Alanine is the smallest and most uncomplicated amino acid participant of molecular biosynthesis. Its molecular structure $CH_3CH(NH_2)COOH$ consists of a carboxylic group (COOH), an amino (NH_2) group, a methyl (CH_3)

group and a hydrogen atom, all bound to a central carbon atom. Due to this methyl group, alanine can be distinguished from other amino acids. There are two isomeric forms of alanine: L- and D-alanine. Combining the two isomers results in LD-alanine. L-alanine and DL-alanine are used the most in dosimetry [36].
When the alanine comes in contact with ionizing radiation, this causes a chain reaction that induces radical production. The most stable radical corresponds to the breaking of the NH_2 group bound. Thereby, an unpaired electron is created, which can be seen in Figure 3. This unpaired electron induces the paramagnetic properties of this amino acid, so it can be read with electron spin resonance. is responsible for the central and most intense line of the spectrum (Figure 4).

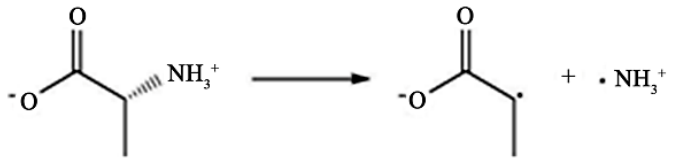

Figure 3: De-amination reaction of L-alanine via homolytic bond cleavage process to form stable radical anion $CH_3CHCO^-_2$ by ionization energy [30, p123].

An EPR spectrum, for example in Figure 4, is formed by a central line with a greater amplitude, caused by the unpaired electron after breaking the NH_2 bound, and with four adjacent lines with smaller intensity due to hyperfine interactions of the unpaired electron with the four hydrogen atoms present in the radical CH_3-C·O-COO. In this way, the number of paramagnetic centers created by ionizing radiation can be detected by an EPR spectrum.

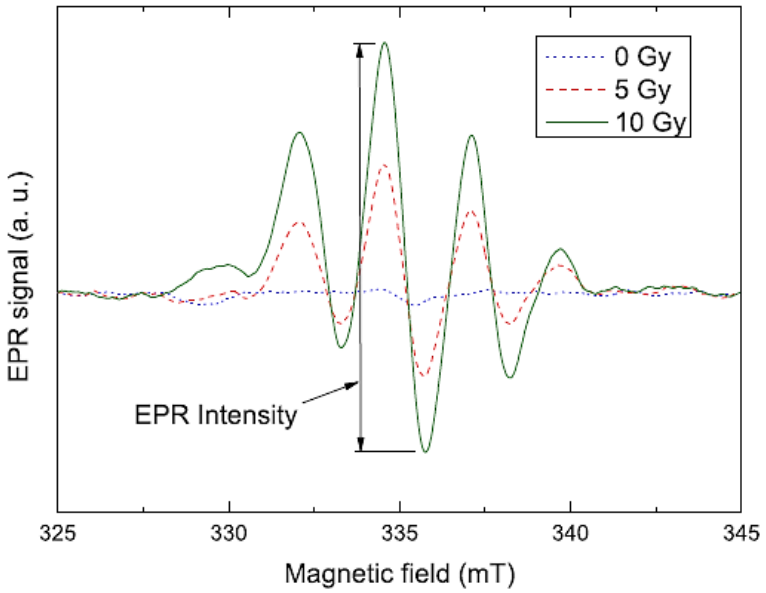

Figure 4: EPR spectra of alanine dosimeters irradiated with photon dose of 5 and 10 Gy. The spectrum of an unirradiated alanine pellet (0 Gy) is added as a reference [29, p430].

Thus, EPR dosimetry is based on the quantification of the concentration of unpaired electrons produced by the interaction with ionizing radiation. The EPR spectrum is recorded by the first harmonic signal of the absorption line under certain conditions. When the modulation amplitude and the microwave power are kept constant in all measurements, the amplitude of the central line in the spectrum can be directly associated with the dose. The behavior of the dose response for alanine for a wide dose interval from a few Gy to 100 kGy is linear.

A small uncertainty in the measurement of the applied dose is possible. By simultaneous read out of the alanine pellets with a reference substance, corrections were made to eliminate temporal variations in the sensitivity of the spectrometer. When the irradiation and read out process is done carefully, the achieved precision can be as low as 0,5 % for doses in the therapeutic range (5-25 Gy). There are two major factors that might affect the amplitude of a radiation induced EPR signal: first of all, the background signal and secondly, the temporal evolution of the signal. This last factor can be caused due to variations in environmental conditions such as the ambient room temperature and the humidity [39],[36]. The indicated response reduction of an alanine-EPR dosimetry system is 0,8 % ± 0,5 % in the therapeutic dose range for photon beams with energies from 10 to 30 MV [40].

Alanine can be used as a transfer dosimeter. The International Atomic Energy Agency (IAEA) chose alanine, among various other dosimeters, as dosimeter in the program of standardization of high-dose measurements because of their subsequent features: (i) alanine has temporal stability, which means there is only little EPR signal fading over time, (ii) alanine requires no special treatment before or after irradiation, and (iii) the read out process makes no changes to the alanine whatsoever and thus the pellets can be saved and read out later for posterior reassessment if necessary [36].

Because of these all the features mentioned earlier, the EPR/alanine system is being applied successfully for medical dosimetry.

3. Method and materials

The practical study involves two large parts. First, the dose differences in between the two calculation algorithms of the TPS (AAA and Acuros) will be investigated. Hereby, the dose differences of the two dose reporting methods of Acuros XB, DTW and DTM, will also be examined. Secondly, the dose differences of the actual treatment and the recalculated dose map of the TPS (for the two available algorithms) will be studied more in detail.

In the Limburgs Oncologisch Centrum (LOC) in Limburg, patients with early stage lung (T1 and T2N0) cancer and lung metastases are treated with SBRT. On Campus Virga Jessa (Hasselt) the TrueBeam® Radiotherapy System is used, while on Campus Genk the type Clinac® iX System Linear Accelerator is operative for SBRT patients. Lung irradiation plans operate on two 6 MV beam arcs and sometimes an additional 6 or 15 MV fixed beam. The arcs on the TrueBeam are FFF, while the arcs of the Clinac in Genk are with flattening filter.
All results of the plan recalculations are based on patients treated in the LOC.

3.1. Plan recalculations

3.1.1. SBRT in clinic

All patients have a 4DCT and are treated in free breathing mode. There is no equipment for gated irradiation or tumor tracking, and irradiation with breath hold is only performed in conformal EBRT treatment.
The planning and delineation of the OAR and target volumes is done on a projected structure set of the 4D planning CT, the maximum intensity projection (MIP). This structure set is a compilation of the GTV in all breathing phases, which represents a projection of all tumor positions in the breathing cycle of the patient. In this case, the delineated tumor volume, i.e. the PTV, does not only contain the GTV plus margin, but also includes lung tissue surrounding the tumor. For peripherally situated tumors, the PTV could also cover a part of the chest wall, with or without a rib structure.
Patients with centrally located tumors (tumors situated near the aorta wall, heart wall or central zone of the bronchial tree [1]) impose extra challenges. When the tumor is situated nearby OAR, the dose fall-off cannot be decreased sufficiently to give fractionation doses >10 Gy. If the TPS cannot meet the prescribed dose constraints for OAR with sufficient target dose, the fractionation scheme is adjusted with more fractions of a lower dose to spare the OAR (lower BED). A number of fractionation schemes are used in the LOC to combine the most qualitative dose-response while taking the dose constraints and toxicity risks for the OAR in consideration. The different fractionating schemes are displayed in Table 1.

Table 1: Fractionation schemes for SBRT lung treatments used in the LOC.

Lung (stage I/II)		
Fractionation schemes	Total dose	Number of patient plans
11 X 5 Gy	55 Gy	1
8 X 7,5 Gy	60 Gy	3
3 X 12 Gy	36 Gy	1
4 X 12 Gy	48 Gy	28
3 X 18 Gy	54 Gy	14

Dose calculations are performed on an average of the 4DCT. In this way, all projections are being considered without overestimating the delivered dose to the PTV and OAR.

3.1.2. Acuros XB vs. AAA

In cooperation with LOC, existing patient plans generated using AAA (version 13.6.23) in Eclipse TPS that were already being used for SBRT treatment, were recalculated with the Acuros algorithm (version 16.6.23) for the dose-to-water as well as the dose-to-medium reporting method. The only effective variable was the difference of calculation algorithm. Other variables such as the dose calculation system, beam setup and prescribed dose were fixed because of an identical setup.
The first purpose of this study is to evaluate the dose distribution of Acuros using two dose reporting modes, compared to AAA, in the cases of lung SBRT with volumetric intensity modulated radiotherapy (VMAT) plans [18]. The currently widely used AAA is known to overestimate dose at the air-tumor interface and underestimate dose at the bone-tumor interface [23]. For 4-6 MV beams and field sizes $\geq$ 5x5 cm², AAA tends to underestimate the dose in lung and overestimate the dose in water-equivalent tissue after the lung [23].
The aim of these recalculations is to examine the dose impact of Acuros XB dose calculation algorithm in lung SBRT. We hypothesize that the tumor volume and the number of beams used in SBRT will influence the difference in target dose distributions calculated by Acuros and AAA.
The target volumes and delineated OAR that were evaluated are shown in Table 2.

Table 2: All delineated areas that were used for data collection and evaluation.

Lung
PTV
SPINAL CORD
ESOPHAGUS
HEART
AORTA
LUNG SUM

In order to collect the needed data, a minimum of 60 patient plans were recalculated with Acuros, both AXB_W and AXB_M. In total, an amount of 63 patient plans for lung were recalculated for AXB with the use of the Eclipse TPS at the LOC.

For dosimetric evaluation, the concerned target volumes (PTV) and other nearby organs at risk (OAR) were compared. The differences between AAA and Acuros (AXB_W and AXB_M) were statistically calculated with a paired t-test and the percentage differences between AXB_W and AXB_M were plotted in a histogram [18].

The lung plans were originally normalized on different base lines that vary from 90 % up to 95 % of the dose on 99 % of the target volume. To be able to compare dose metrics the plan normalization was set off. They were recalculated with fixed MU.
Since AAA is currently being used in the clinic, this algorithm will be used as the standard in this study to which the other algorithms are compared.

3.2. Dose verification with a phantom

3.2.1. Virtual Water IMRT Dose Verification Phantom

The Virtual Water™ IMRT Dose Verification Phantom© (Standard Imaging, Wisconsin, USA), depicted in Figure 5, can be used for quality assurance of a linear accelerator. The phantom consists of six tissue equivalent (Virtual Water™ REF 91235 material) slabs, of which two slabs have cavities for lung inserts. Furthermore, the phantom has a bone equivalent plug to simulate the spine. A set of four lung-equivalent inserts is also included, which can be replaced with ion chambers for dose measurement. In this study, no ion chambers are used.
The individual lung inserts can be removed or partially replaced by 3D printed structures. This makes it possible to personalize the phantom for one case or patient as well as to compare dose distributions in between real patient plans and the Virtual Water IMRT Dose Verification phantom.
For dosimetry purposes, the phantom is accommodated with six plugs that can be replaced by ion chambers and radiochromic films can be placed in five different positions between the slabs [41].
With its anthropomorphic design, the IMRT Dose Verification Phantom mimics robustly the human anatomy. Also, the accuracy of the prescribed dose is evaluated and confirmed in simulated patient conditions. Due to its material characteristics, anthropomorphic design and flexible slab set up, this phantom is ideal for patient dose verification [41].

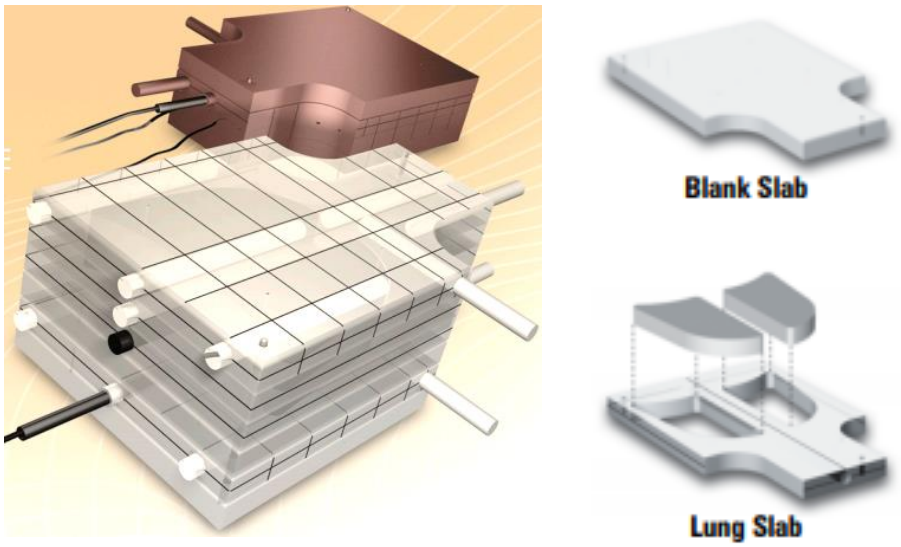

Figure 5: Virtual Water IMRT dose verification slab phantom of Standard Imaging © [22, p 1]

3.2.2. Dose verification using a phantom with hydrogel tumor

In cooperation with the BEL*d*ART (Belgian dosimetry audit in radiotherapy team), the accuracy of the AAA and Acuros algorithm will be tested with the IMRT dose verification phantom of Standard Imaging.
A part of the lung is replaced with a box, 3D printed with a low infill PLA, that is lung equivalent. The 3D printed box has an imprint based on patient contours of a lung tumor and inside this shell, a hydrogel substance mimics tumor tissue. With this phantom, BEL*d*ART wants to use this phantom to develop an End-To-End (E2E) test which will part of their future lung SBRT external dosimetry audit procedure.

Two dosimeters with complementary properties were chosen for dose measurements. L-α-alanine to provide accurate, small volume dosimetry at the target volume center and EBT3 GafChromic™ film (Ashland, Covington, USA) to provide high resolution planar dosimetry, thereby measuring the dose coverage of the target volume and the surrounding dose fall-off in normal lung tissue. Both measurements correlate with clinically important parameters: dose at the PTV center (tumor control probability) and dose coverage around the PTV (irradiation of surrounding tissue relates to normal tissue effects). For the PTV, a simultaneous measurement using the two dosimeters was chosen to provide a thorough, clinically relevant and practical method. Practically, this means that an alanine pellet and an EBT3 film was placed at the center of the tumor. However, high accuracy in dose prediction to the PTV does not necessarily mean that organs at risk (OAR) dose prediction is also accurate, so 2D dose measurement was done, using EBT3 films, above the tumor and at the center of the tumor with an EBT3 film size of approximately 10x10 cm² [42].
The radiation dose is measured using a combination of L-α-alanine (Harwell Dosimeters LTD, Oxfordshire, UK) EMR dosimetry and radiochromic EBT3 films (lot #03211802). The films are read using the 'One-scan' procedure [26] and triple-channel dosimetry in the FilmQA Pro software developed by Ashland [1].

3.2.3. Phantom testing

Lung equivalent material

The IMRT dose verification phantom consists of 6 individual slabs with a thickness of 3 cm each. All slabs are made of virtual water. Two out of six slabs have voids that can be filled with lung equivalent inserts. Also, a bone equivalent plug for the spine can be inserted.
As Figure 6 shows, a square cavity of 4x4x1,5 cm³ is present in two lung slabs. With these voids, the possibility exists to make the phantom patient specific, except for the position of the tumor in the lung.

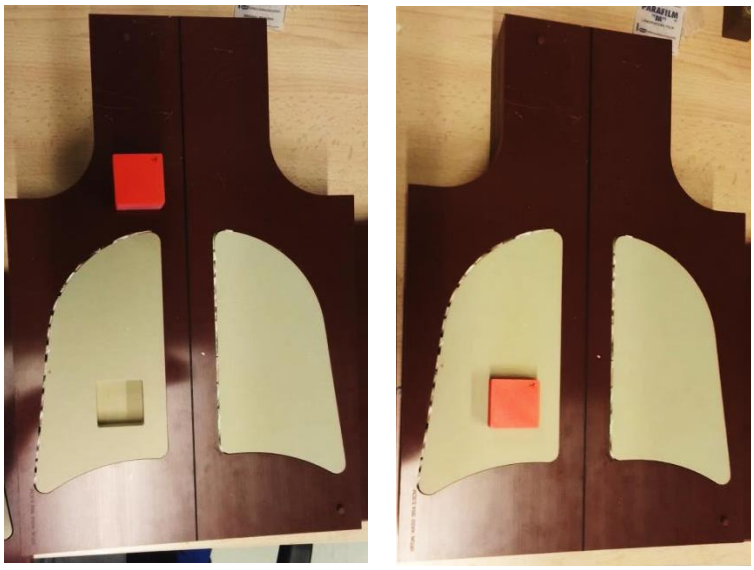

Figure 6: IMRT dose verification phantom with lung equivalent 3D printed box (red)

Using 3D printing, the voids can be filled with two square boxes that encapsulate a reproduction of a patient's tumor in hydrogel. The boxes that fill the void, and a tumor example can be seen in Figure 7 below.

Figure 7: Example of 3D printed lung equivalent boxes, with hydrogel tumor.

To realize this patient-specific phantom set up, tissue equivalence tests were performed for both the 3D printed box and the tumor.

To simulate lung tissue using polylactic acid (PLA) in a 3D printing process, three boxes were printed in Maastro Clinic, Maastricht, NL. The settings for the three boxes were varied, as depicted in Figure 8 below. The three boxes were fabricated with the purpose of varying the mass density while maintaining chemical composition, using only a low atomic number element as in organic tissues. In this way, phantom inserts can be developed that accurately model the attenuation of lung tissue.

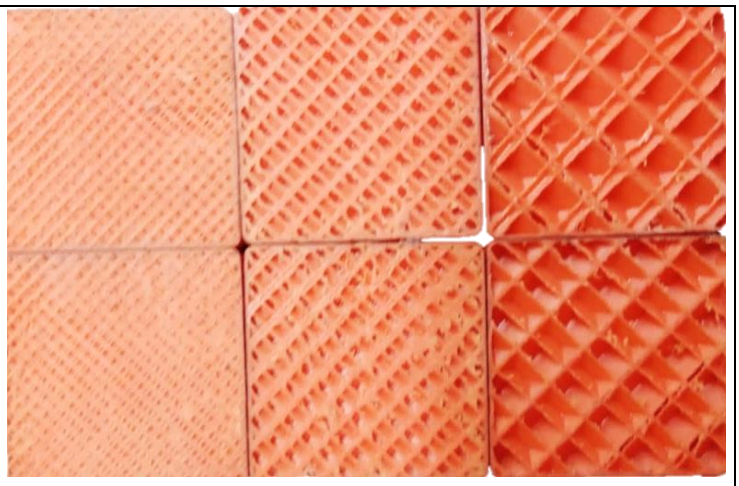

	Nr 1	Nr 2	Nr 3
PLA infill (%)	40%	40%	20%
Line width (mm)	0,2	0,4	0,4

Figure 8: The inside structure of the infill of the three 3D printed boxes that were assessed for tissue equivalence of lung.

First, the phantom with each 3D printed box was CT-scanned at LOC to evaluate the lung equivalence of the box, compared to the lung inserts of the phantom. The structure, the density and Hounsfield Units (HU) were evaluated.

After comparison of the profiles in Eclipse (Varian), box nr.1 with the lowest grade of infill and finest printing nozzle appeared to have the best profile.

Afterwards, the phantom was irradiated three times, each time containing a different box, with an EBT3 film piece underneath the lung slab. The linac irradiated the phantom with a static 6 MV photon beam at a field size of 10x10 cm^2 (1000 MU, 600 MU/min). The films were read out with a high-resolution flatbed scanner at NuTeC. Using the FilmQA Pro software (Ashland, Covington, USA), a horizontal dose profile of each irradiated film was taken and compared to an irradiated film positioned beneath the already present lung inserts of the Virtual Water Dose Verification phantom. In this way, the effect of the material on the dose for each box and the already present lung insert material can be compared.

3.2.4. Tumor equivalent material

After successfully finding an alternative lung equivalent material, a tumor equivalent material to fill the void inside the 3D printed boxes was explored. Since a lung tumor originates out of normal, healthy tissue, their material equivalence is very similar. Therefore, a soft tissue equivalent material needed to be found. Normal tissue is often simulated with (virtual) water or water equivalent slabs. Consequently, replacing tumor tissue with a water-based material, such as hydrogel, was found to be a realistic alternative.

The density of lung tumors can vary from 0,236–1,010 g/cm^3 (mean: 0,697 g/cm^3) [43]. Based on this density, three different ratios of water and gelatin were considered as tissue equivalence, as seen in Table 3. The three hydrogels were scanned on CT and afterwards irradiated with a linac.

Table 3: Types of hydrogel tested as tumor equivalent material.

	Hydrogel 1	Hydrogel 2	Hydrogel 3
Gelatin water ratio (%)	10,5	15,0	19,0

The gelatin water ratio of 10,5 % was chosen as the best fit for a tumor equivalent material.

3.2.5. Final clinical set up

Figure 9 displays the final set up of the phantom. The red box is the 3D printed tumor shell, filled with a white hydrogel tumor. The two black lines represent the two EBT3 radiochromic films and the blue box at the tumor center represents the alanine pellet.

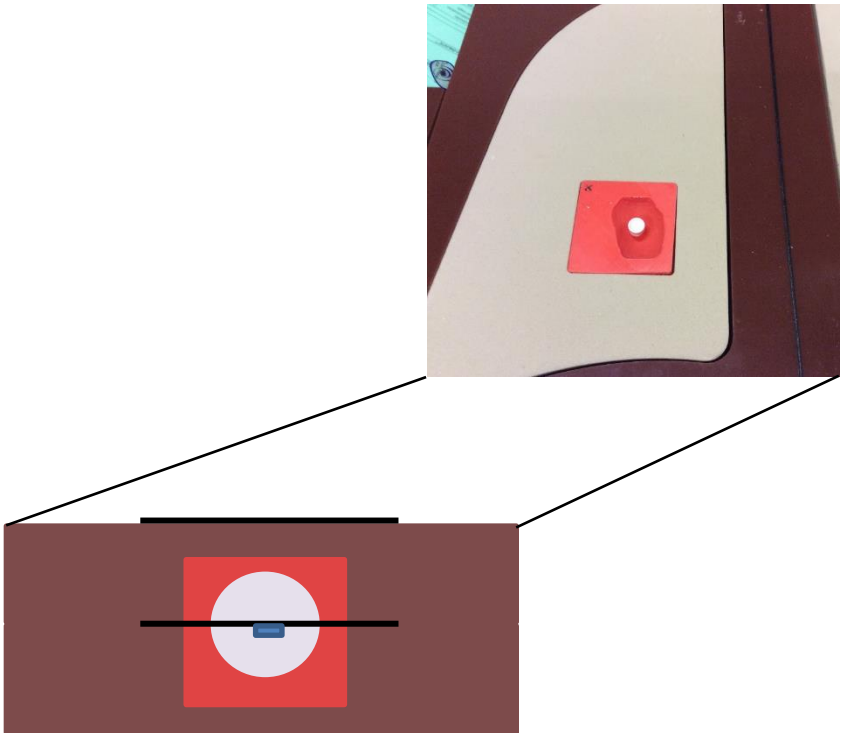

Figure 9: The final set up of the patient specific phantom used in this study.

3.2.6. Patient specific phantom tests

Three separate dose measurements were performed using the IMRT dose verification phantom.

As a first test, the phantom was scanned using a CT and the tumor volume, alanine and body of the phantom were delineated. The phantom was irradiated with three static beams, each with a field size of 5x5 cm^2 at an energy of 6 MV and a dose rate of 600 MU/min. The phantom received a total dose of 12 Gy.

A second test consisted of irradiating the phantom with a more complex plan. The phantom was scanned using a CT, and the tumor volume, alanine and body of the phantom were delineated. Two of the tissue equivalent plugs were delineated as an esophagus structure and the aorta, the spine rod was delineated as well and assigned as the spinal cord. The phantom was irradiated with the total plan dose (3 fractions of 18 Gy) of 54 Gy using two arcs of 6 MV (FFF) arcs for a total dose of 54 Gy (3 fractions of 18 Gy).

For the last test, another patient's lung tumor was used in the phantom. The method is similar to the second phantom test. It only contains a different hydrogel tumor, and thus the irradiation plan is different. The phantom was scanned, the tumor volume, alanine and body of the phantom were delineated. Two of the tissue equivalent plugs were delineated as an esophagus structure and the aorta, the spine rod was delineated as well and assigned

as the spinal cord. The phantom was irradiated with 2 6 MV (FFF) arcs for a total dose of one fraction of 18 Gy.

The phantom has the exact same set up in all the three patient specific dose measurements. In all three measurements a different tumor was used, and nearby OAR (esophagus, aorta and spinal cord) were delineated nearby, to make the phantom more realistic. The plans delivered to the phantom were all calculated with AAA, the standard algorithm used in the LOC, and afterwards recalculated for AXB_W and AXB_M.
Next, the dose maps of AAA, AXB_W and AXB_M were compared to the dose of the films. The two EBT3 films of each phantom test were read out 24h after irradiation.
For each irradiated film a horizontal dose profile was extracted from the Film QA Pro software at film height (center of the tumor and above the tumor). Also, a gamma analysis was performed to compare the dose of the TPS, calculated for AAA, AXB_W and AXB_M, with the films.

3.2.7. Dose constraints

The LOC follows dose constraints for the OAR, as proposed by the Radiation Therapy Oncology Group and the European Organization for Research and Treatment of Cancer. These constraints, as seen in Figure 10, were also applied to calculate the three phantom specific plans.
Next to these dose constraints for the OAR, the LOC handles an upper dose limit for the PTV, when calculating the dose plan. The maximum dose received by the PTV must be lower than 140 % of the fraction dose. Since the dose constraints of the OAR have a higher priority, this mostly leads to a maximum dose received by the PTV of 130 % of the fraction dose.

Organ at risk	3 fractions (RTOG 0618)	4 fractions (RTOG 0915)	5 fractions (RTOG 0813)	8 fractions (LungTech trial)
Spinal cord	D_{max} 18Gy	D_{max} 26 Gy 20.8 Gy <0.35cc	D_{max} 30 Gy 22.5 Gy <0.25cc	D_{max} 32 Gy
Esophagus	D_{max} 27 Gy	D_{max} 30 Gy 18.8 Gy <5cc	D_{max} 35 Gy[a] 27.5 Gy <5cc	D_{max} 40 Gy
Heart	D_{max} 30 Gy	D_{max} 34 Gy 28 Gy <15cc	D_{max} 38 Gy[a] 32 Gy <15cc	0.5cc <63 Gy 38 Gy <15cc 27 Gy <33%
Brachial plexus	D_{max} 24 Gy	D_{max} 27.2 Gy 23.6 Gy <3cc	D_{max} 32 Gy 30 Gy <3cc	D_{max} 38 Gy
Lungs	V20 <15%	V20 <15%[d]	V20 <15% [d]	V20 <15% [d]
Trachea & large bronchi	D_{max} 30 Gy	D_{max} 34.8 Gy 15.6 Gy <4cc	D_{max} 38 Gy[a] 18 Gy <4cc	D_{max} 44 Gy
Aorta, large vessels	D_{max} 45 Gy[a] 39Gy <10cc[a]	D_{max} 49 Gy 43 Gy <10cc	D_{max} 52.5 Gy 47 Gy <10cc	-
Skin	D_{max} 24 Gy	D_{max} 32 Gy 30 Gy <10cc	D_{max} 36 Gy 33.2 Gy <10cc	-
Chest wall	27.3 Gy <2cc[b]	30 Gy <30cc[c] 60 Gy <1.4cc[c]	30 Gy <30cc[c] 60 Gy <1.4cc[c]	-
Contralateral lung	*V5 as low as possible: ideally 0%, should not exceed 15%*			

Figure 10: Dose constraints for SBRT plans applied in the LOC.

3.2.8. Dose verification with alanine and EPR

The irradiated L-alanine pellets were read out at NuTec using an Electron Paramagnetic Resonance spectrometer (Bruker EMX^{micro} spectrometer (9'' magnet, X-band) equipped with a high sensitivity resonator ER4119-HS-W1). The L-alanine is chosen since it has a higher EPR signal than the D-isomer. EPR spectra were acquired as the first derivative of the absorption spectrum using the following spectrometer settings in Table 4:

Table 4: EPR spectrometer settings used to read out the alanine.

Centre magnetic field	348 mT
Sweep width	30 mT
Microwave power	0,25 mW
Field modulation	0,5 mT
Modulation frequency	100,00 kHz
Conversion time	40.96 ms
Sweep time	83.89 s
Number of channels per sweep	2048

Prior to read out, the pellets were weighed individually, and the response was adjusted for variations in mass. The spectrometer was operating in an air-conditioned room which temperature and relative humidity (RH) were permanently monitored (T≈21 °C, RH ≤ 40 %). To rule out possible angular dependency, five separate spectra were acquired for each detector after subsequent equal rotation steps. Temporal variations in the spectrometer sensitivity were corrected for by recording the irradiated alanine spectra simultaneously with a reference substance, chromium. The dose of the alanine/EPR was calculated using a custom Matlab code from the primary standard lab, Physikalisch-Technische Bundesanstalt, in Braunschweig, Germany [44].
Data acquisition, manipulation, and visualization were fully computer controlled by Software from Bruker (Billerica, MA, USA).

3.2.9. Dose verification with radiochromic EBT3 film

The currently used approach in this study for dose delivery quality assurance consists of delivering the IMRT plan to an IMRT dose verification phantom of Standard Imaging and then comparing the 2D dose distribution calculated by the TPS with the value measured by radiochromic EBT3 films and L-α-alanine pellets.
The 3D printed boxes with imprint of the tumor are filled with hydrogel before scanning. An EBT3 radiochromic film will be placed in between the two 3D boxes. An alanine pellet will be placed inside the gel in the center of the artificial tumor.
To protect the alanine pellet of contact with the hydrogel, a small cover was 3D printed in PLA. While the hydrogel was only set partially, the PLA cover was placed carefully in the center of the hydrogel. Before scanning, the alanine was placed in the PLA cover set in the hydrogel.
The films were handled according to the procedure outlined in the American Association of Physicists in Medicine (AAPM) TG-55 Report [45] and all used films originated from the same lot (lot # 03211802). Each film sheet was cut into a 10x10 cm² pieces and placed in between the two hydrogel filled 3D boxes. The films were irradiated during the entire SBRT treatment. The film pieces were carefully positioned to ensure same orientation on the central axis of the IMRT dose verification phantom at a depth of 7,5 cm (1,5 cm above the tumor) and 9,0 cm (in the center of the tumor) in the coronal plane.

Exposure to light was minimized by keeping the films in lightproof envelopes when they were not being handled for exposure or scanning.

Establishing a calibration curve for EBT3 gafchromic films

A calibration curve needs to be established so the dose of the irradiated films can be read out precisely. Therefore, 8 film pieces were cut out of a film from the exact same box as all used radiochromic films. Eight film pieces of 8x3 cm² were irradiated, all with different doses: 0, 1, 2, 4, 8, 16, 32 and 64 Gy. The film pieces were irradiated at an SSD of 100 cm with a 10x10 cm² field, as depicted in Figure 11.

To adjust the dose of the film, 4 alanine pellets were irradiated, simultaneously with a film piece, to limit the uncertainties on the film calibration. The 4 alanine pellets were situated at 10 cm depth, in a virtual water slab phantom when they were irradiated with a 6 MV static beam at a 10x10 cm² field. The 4 pellets were read out with an EPR spectrometer to determine the absolute dose of the beam and adjust the dose to the irradiated films.

Figure 11: Set up of film calibration with the TrueBeam linac at Jessa Hospital.

Scanning protocol and analysis

An Epson Expression 10000 XL document scanner, with its associated software, EPSON SCAN v3.04, was used. The scanner was set to transmission mode with a 48-bit TIFF image (16 bits per channel), scan resolution of 72 dots per inch (dpi), professional mode, with all available image correction methods turned off. All film pieces were read out at least 48h after irradiation, removing the largest post-irradiation changes which occur within the first twelve hours were positioned at the same location in the center of the scanning area. To reduce the effect of the lateral dependence artifacts to a minimum (the irregular response of the readout caused by light scattering of the scanner lamp due to small fragments in the film), a cardboard template (with rectangular hole for the films) was fitted to the scanner, not only to reduce lateral scan artefacts, but also to position films at a reproducible central location of the scan surface that can be considered uniform. Additionally, a glass sheet to compress the films avoids film curvature during scanning.

Individual channel values were extracted by using Film QA Pro software. A 2x2 cm^2 region of interest (ROI) at the center of each film was selected. Data was obtained for the red, green and blue color channels at a resolution of 16 bits per channel.
Data and image analysis such as reconstruction of images from scanner space to dose space and measurement of film profiles was also performed with the Film QA Pro software. This application has a utility for calculation dose images using triple-channel dosimetry.
Photon beam irradiation with beams of 6 MV (dynamic arcs) were performed using a TrueBeam® and Clinac® Linear Accelerator (Varian Medical Systems).

Uncertainty analysis

When considering all uncertainty parameters, a total estimation of the uncertainty of the results can be made. Taking into account a total uncertainty of 1 % for the film, and 0,5 % for the alanine, a total uncertainty of the dosimetry system can be made: $\sqrt{1^2 + 0{,}5^2}$= 1,1 %.
Certainly, this is the minimum total uncertainty that can be accounted for. Other human errors can increase the uncertainty, but since a quantitative measurement was not performed in this study, this contribution to the uncertainty is not known.

4. Results

4.1. Recalculation of patient plans

First, the relative and absolute mean differences of the dose parameters, normalized to the used standard AAA in this study, were compared and graphically plotted with addition of the standard deviation.
A t-test was subsequently carried out to either confirm or deny the relation between AAA and AXB_M and AAA and AXB_W on a significance level of a < 0,05. These results can be found Table 5 below. The null hypothesis states that the sample derives from a normal distribution corresponding with the calculated mean and standard deviation. If not, the alternative hypothesis states the sample does not derive from this.
In addition to testing the relevance of the executed comparison between algorithms, the absolute percentage differences are reviewed. Clear deviations can be seen for the PTV, spinal cord and skin.

Figure 12 displays the results of the plan recalculations for the delineated volumes in lung SBRT. For the PTV, spinal cord and skin, AAA overestimates the dose by approximately 5-6 %, according to Acuros (both AXB_M and AXB_W. For Lung sum, esophagus and the heart, AAA underestimates the dose with 0,3-2,20 %. For the aorta, there is an overestimation of AAA dose for 1-1,90 %, compared to Acuros.

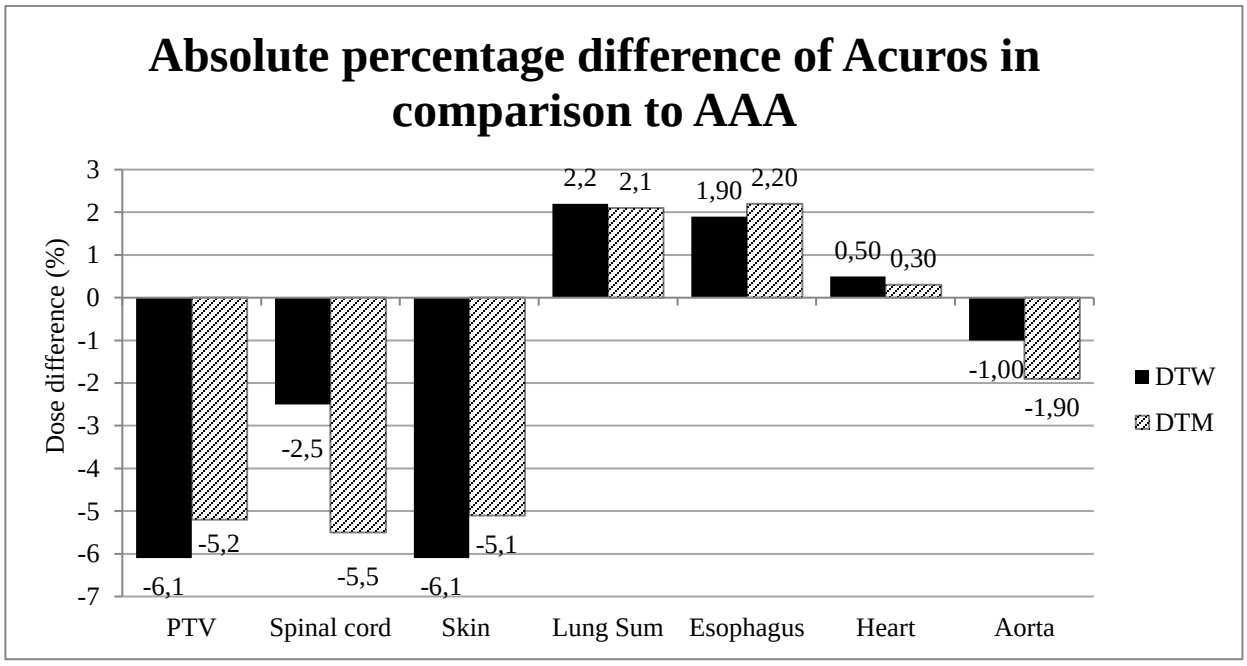

Figure 12: Absolute percentage difference of AXB_M and AXB_W in comparison to AAA for all delineated volumes.

The t-test for PTV, shown in Table 5, spinal cord, lung sum and skin show values which are lower than the significance level of 0,05. For the other delineated volumes (Esophagus, Heart and Aorta) the t-test results were higher than the significance level.

Table 5: T-test significance between AAA and AXB_W, AAA and AXB_M, AXB_W and AXB_M for $\alpha = 0,05$ with non-significance colored red.

	T-test between		
	AAA AXB_W	AAA AXB_M	AXB_W AXB_M
PTV	2,02E-02	1,21E-02	5,99E-04
SPINAL CORD	7,14E-02	4,86E-04	5,58E-12
ESOPHAGUS	2,75E-01	1,97E-01	1,49E-01
HEART	6,79E-01	8,19E-01	1,08E-01
LUNG SUM	5,71E-06	3,33E-05	2,52E-05
AORTA	5,09E-01	2,44E-01	2,52E-01
SKIN	2,43E-08	1,82E-06	1,68E-04

4.2. Phantom tests

4.2.1. Lung and tumor equivalence tests

Figure 13 depicts the dose profiles of the EBT3 films placed underneath each 3D printed box and underneath a part of the lung equivalent material used in the phantom. After comparing the dose profiles in FilmQA Pro the dose profile of box 3 showed the best agreement with the dose profile of the lung equivalent material of which the lung inserts consist.

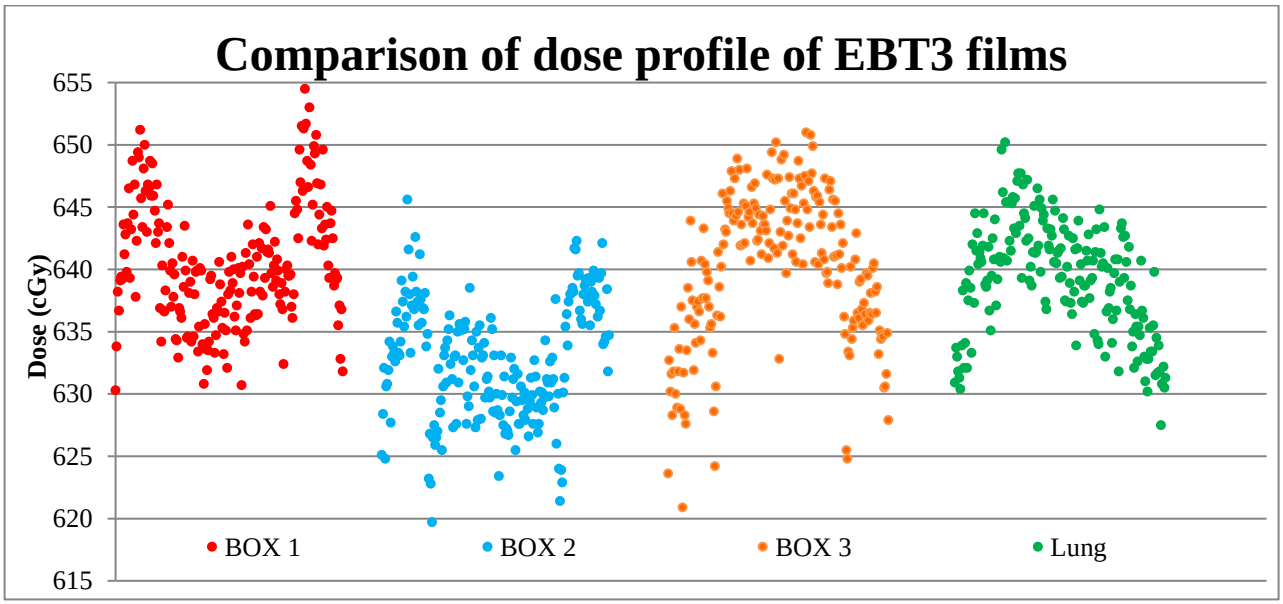

Figure 13: Comparison of dose profiles from the EBT3 films after irradiation of the three 3D printed boxes and the lung equivalent tissue of the phantom.

4.2.2. Alanine

During each phantom test, an alanine pellet was placed in the center of the hydrogel tumor to measure the dose. Afterwards, the pellets were read out and the dose was compared to the TPS, as depicted in Table 6. In the second phantom test, the alanine pellet was contaminated with hydrogel. Therefore, it was not read out to prevent the spectrometer from contamination.

Table 6: The mean dose of the TPS, compared to the dose of the alanine, for AAA, AXB_W and AXB_M.

Test 1: 3 static fields	Algorithm	TPS dose (Gy)	Dose alanine (Gy)	TPS/alanine
	AAA	12.204	11.982	1.018
	AXB_W	12.250	11.982	1.022
	AXB_M	12.180	11.982	1.016
Test 2: 2 arcs	No read out due to contamination			
Test 3: 2 arcs	AAA	22.344	21.693	1.030
	AXB_W	22.427	21.693	1.034
	AXB_M	22.002	21.693	1.014

4.2.3. Calibration

The films of all three phantom tests were read out in the flatbed scanner. A calibration curve was made using the irradiated film pieces with a dose of 0, 1, 2, 4, 8, 16, 32, 64 Gy. All calibration films (0, 1, 2, 4, 8, 16, 32, 64 Gy) used for the calibration curve, can be seen in Figure 14. The calibration curve was adjusted using the linearity of the linac output to extrapolate the dose of 4 irradiated alanine (1600 MU) pellets to the other films, of which the results can be found below in Table 7.

Table 7: The measured dose and the uncertainty on the dose for the 4 alanine pellets used for the calibration.

	Measured dose (Gy)	Uncertainty (Gy)	Uncertainty (%)	N
Calibration 16 Gy	16.04	0.12	0.73	4

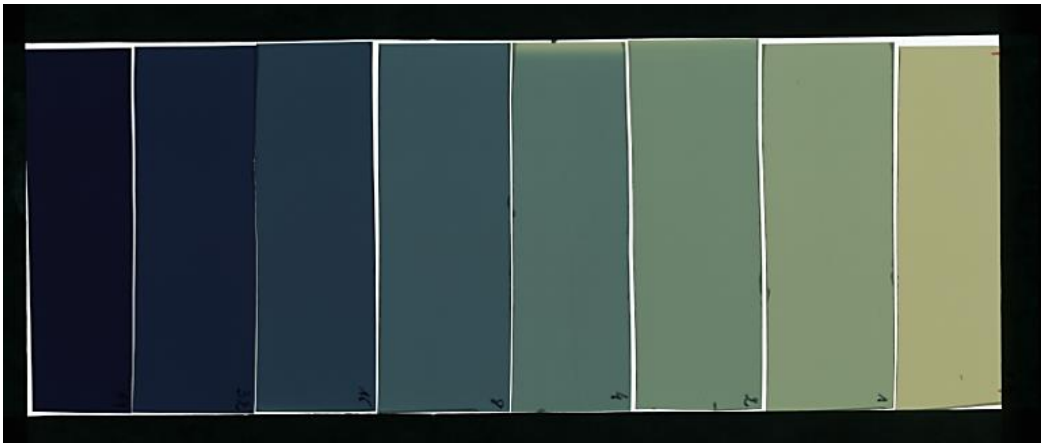

Figure 14: All calibration films (0, 1, 2, 4, 8, 16, 32, 64 Gy) used for the calibration curve.

The films were mapped from image space to dose space using only the calibration curve, and thus without using the one-scan method. The resulting calibration curve is depicted in Figure 15. For the films of test 3, the calibration curve was used, as well as a rescaling using the OneScan method. The OneScan method was applied using the calibration films of 0 Gy and 16 Gy, as visualized in Figure 16 below.

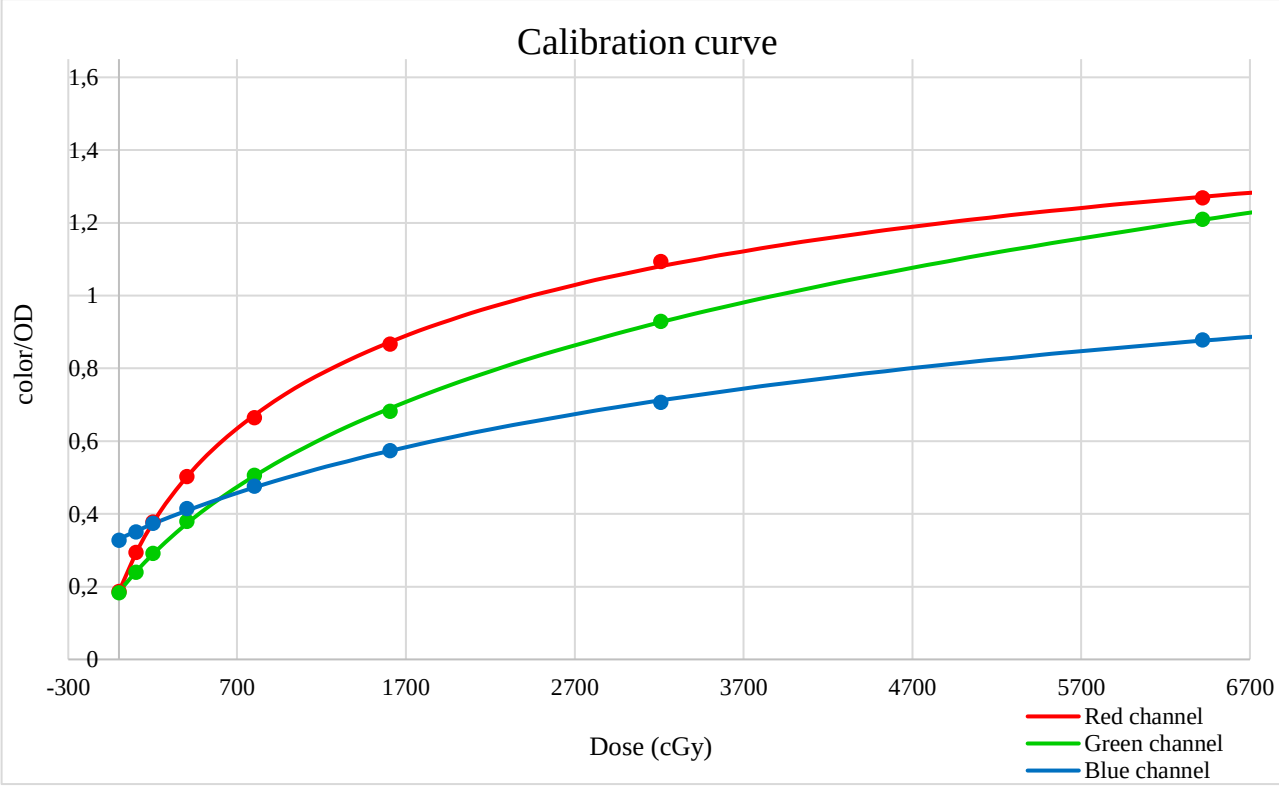

Figure 15: Calibration curve for the green, blue and red channel, based on the irradiated calibration films.

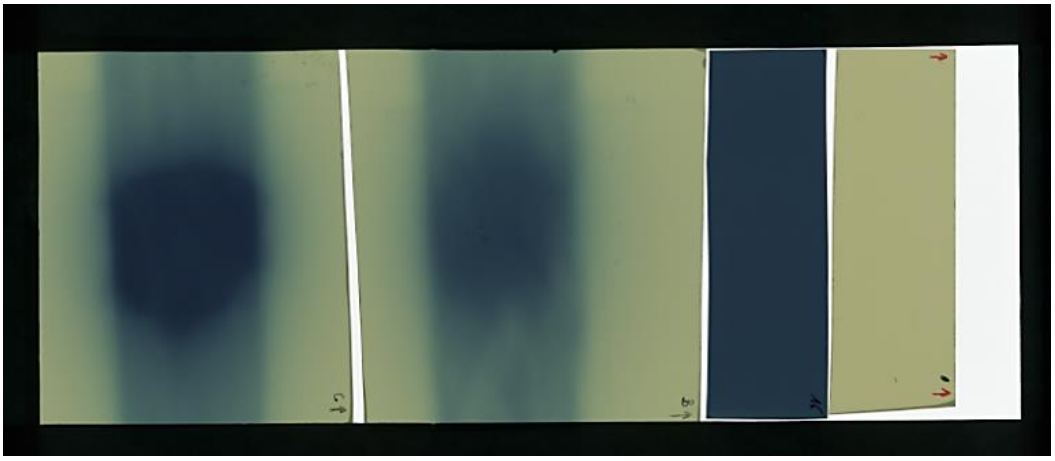

Figure 16: The two films, irradiated in test 3, were scanned simultaneously with the 0 Gy and 16 Gy calibration films, as required for the Onescan method.

The dose profile of the TPS (AAA) was compared to the dose profile of the film, as depicted in Figure 17. A dose difference op up to 300 cGy was noticed between TPS dose and film dose, when using the OneScan method. To ensure that the OneScan caused this dose difference, the mean dose of the alanine calculated by the TPS was compared to the film dose. A significant dose difference only occurs when the films are rescaled with

the OneScan method. When the dose of the film is only calibrated using the calibration curve, the calculated dose of the TPS (AAA) is in proper accordance with the film dose. The good dose agreement of the alanine and the TPS justifies discarding the OneScan method for the film read out. The dose difference of the film without and without rescaling with the OneScan method can be seen in Figure 17.

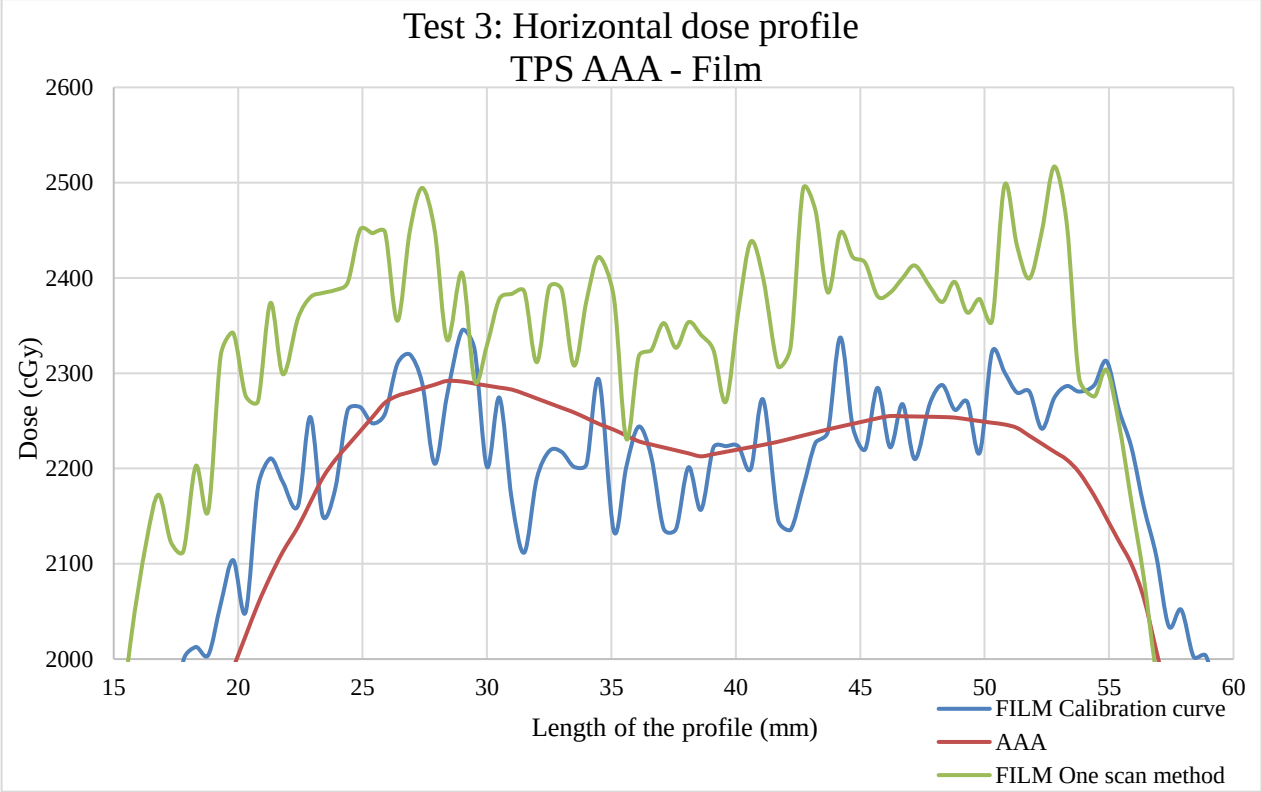

Figure 17: The horizontal dose profile of the TPS (calculated with AAA), compared to the film, calibrated with only the calibration curve (green graph) and calibrated with the calibration curve and rescaled using the OneScan method (blue graph).

4.2.4. Phantom tests: general

The criteria of dose difference < 3 % and distance-to-agreement <2 mm were applied for all gamma maps. For this 3 %/2 mm criteria, the passing rate is 99 % at the green channel for the gamma maps at the center of the tumor. A passing rate of 99 % could not be achieved for all gamma maps above the tumor, but a minimum of 88 % was reached for all gamma maps above the tumor.
Additionally, for all gamma maps, the reference image used for the gamma analysis is the image from the dose matrix calculated by the TPS. If the scanned would be taken as the reference, the passing rate would drop because of the increased noise of the film.

4.2.5. Test 1: 3 static fields

Figure 18 depicts the horizontal dose profiles for each calculated dose plan (AAA, AXB_W and AXB_M) compared with the dose of the film, all in the center of the tumor. The dose profiles are given over a length of 50 mm, with the tumor in the center. The dose profiles, calculated for AAA, AXB_W and AXB_M, show all good similarity and are in accordance with the film dose. Furthermore, the maximum dose of 12 Gy in the PTV can also be verified easily.

Figure 19 displays the horizontal dose profiles for each calculated dose plan (AAA, AXB_W and AXB_M) compared with the dose of the film, all at the same height above the tumor, and more specific, at the lung-soft tissue transition. All profiles are in accordance with the film dose. No significant dose differences between AAA, AXB_W and AXB_M can be noticed.

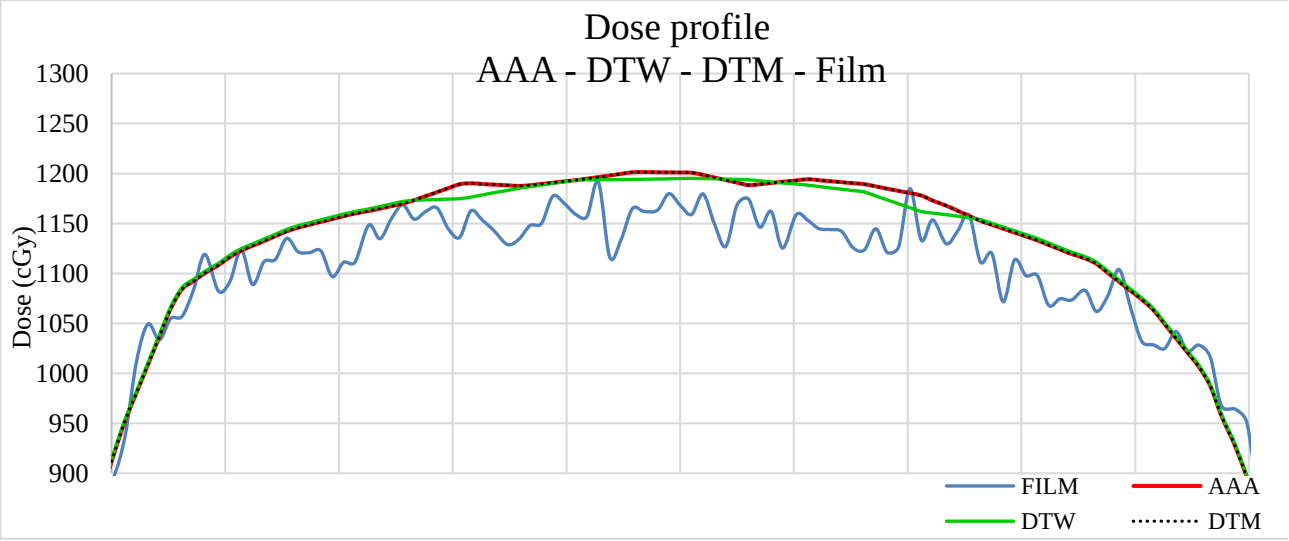

Figure 18: Comparison of the dose profiles for each calculated algorithm (AAA, AXB_W and AXB_M) and the film dose at the center of the tumor.

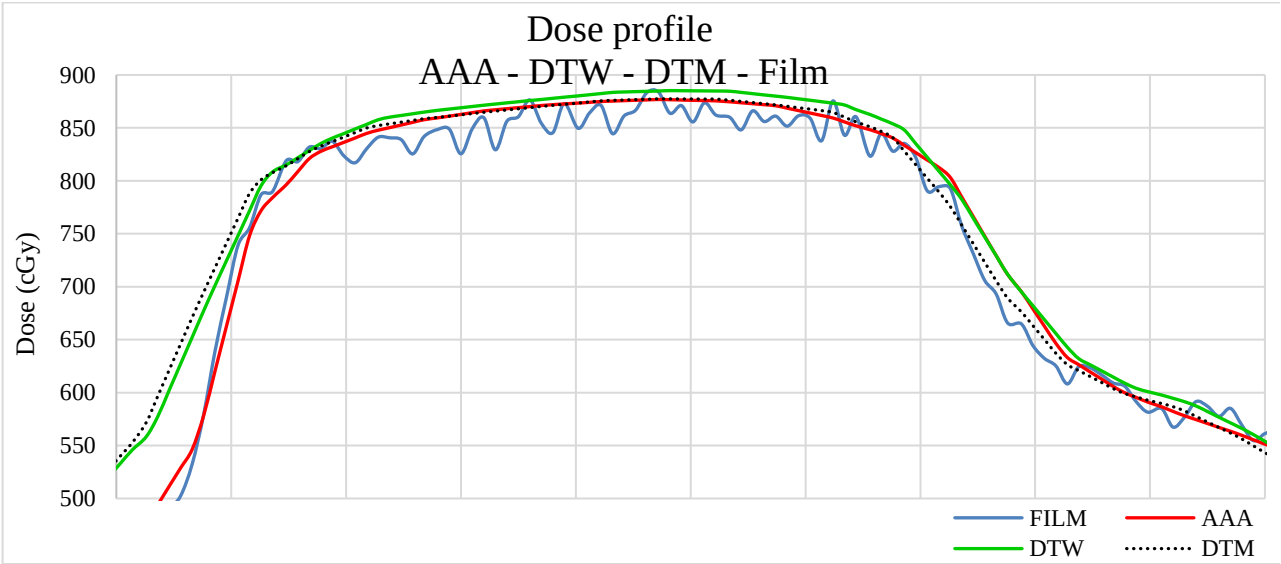

Figure 19: Comparison of the dose profiles for each calculated algorithm (AAA, AXB_W and AXB_M) and the film dose above the tumor.

Figure 20, Figure 21 and Figure 22 display the gamma analysis results for comparing the film dose in the center of the tumor with the recalculated dose of the TPS for respectively AAA, AXB_W and AXB_M.
The gamma analysis of the AAA dose map and the film shows small dose differences over the whole 2D dose distribution, varying from 0,00 % to 1,30 %, based on the legenda provided by the Film QA Pro Software.
The gamma analysis of AXB_W and the film dose (at center of tumor) and AXB_M and the film dose (at center of tumor), show a similar pattern concerning the dose differences. These differences are only minor, from 0,00 % to 1,30 %.

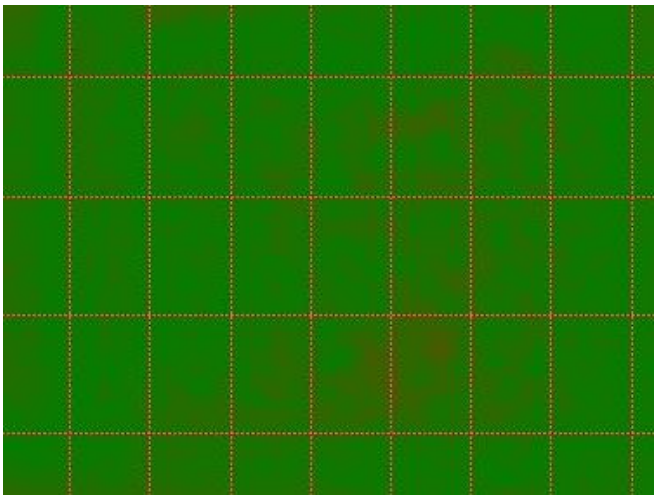

Figure 20: Gamma analysis of film dose and AAA dose map at the center of the tumor.

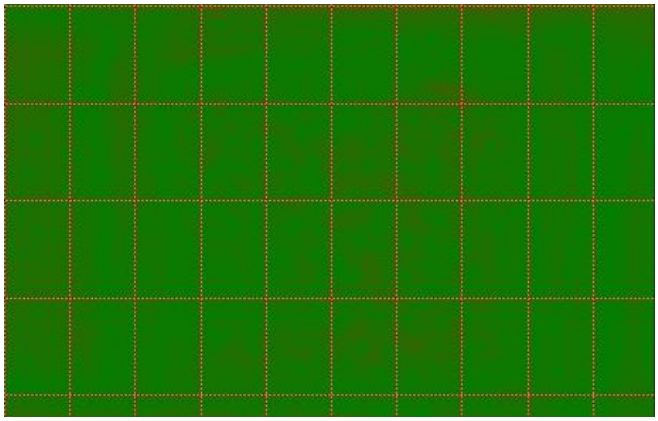

Figure 21: Gamma analysis of film dose and AXB_W dose map at the center of the tumor.

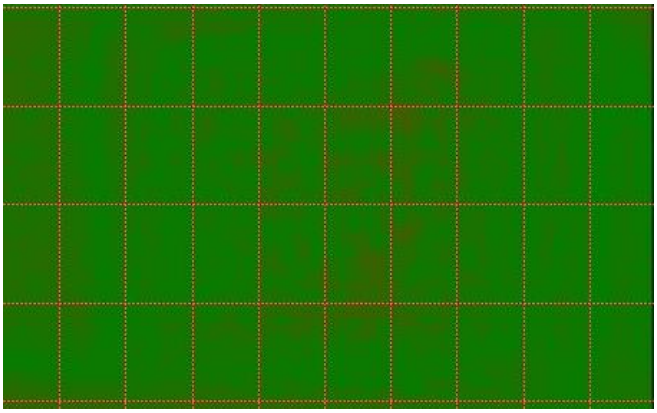

Figure 22: Gamma analysis of film dose and AXB_M dose map at the center of the tumor.

Figure 23, Figure 24 and Figure 25 display the gamma analysis results for comparing the film dose above the tumor with the recalculated dose of the TPS for respectively AAA, AXB_W and AXB_M.
The gamma analysis of the AAA dose map and the film shows no dose difference over the whole 2D dose distribution that was registered. The gamma analysis of AXB_W and the film dose and AXB_M and the film dose, show a similar pattern concerning the dose differences. These differences in dose vary from 0,00 % to 2,00 %, based on the legenda provided by the Film QA Pro Software.

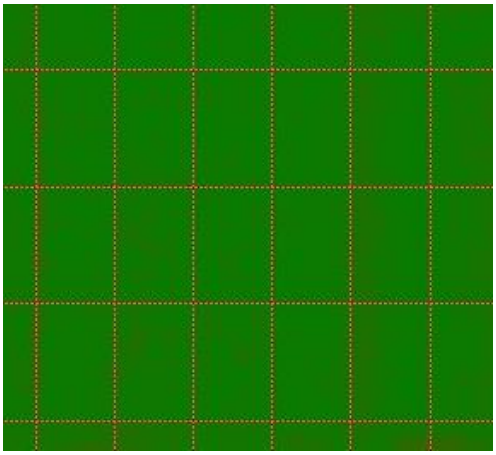

Figure 23: Gamma analysis of film dose and AAA dose map above the tumor.

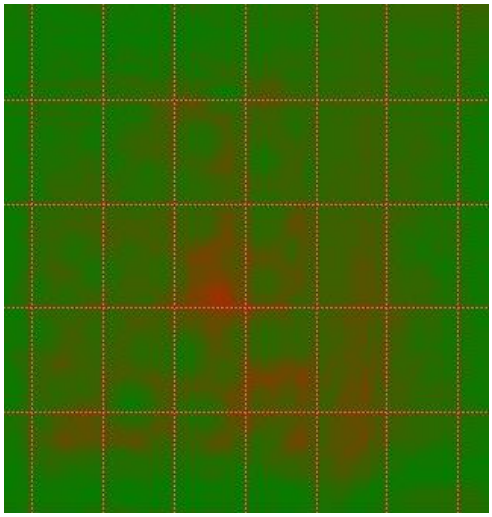

Figure 24: Gamma analysis of film dose and AXB_W dose map above the tumor.

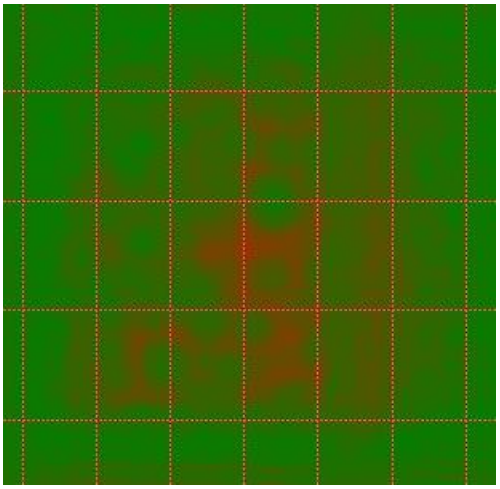

Figure 25: Gamma analysis of film dose and AXB_M dose map above the tumor.

4.2.6. Test 2: 2 arcs

Figure 26 displays the horizontal dose profiles for each calculated dose plan (AAA, AXB_W and AXB_M) compared with the dose of the film, all at the center of the tumor. All profiles are in accordance with the film dose. No significant dose differences between AAA, AXB_W and AXB_M can be noticed. The TPS shows a slight overdosage for all calculated algorithms, compared to the film dose of approximately 1,7 %.
Figure 27 depicts the horizontal dose profiles for each calculated dose plan (AAA, AXB_W and AXB_M) compared with the dose of the film, all at the same height above the tumor, and more specific, at the lung-soft tissue transition. The dose profiles of AAA, AXB_W and AXB_M show an underdosage compared to the film. This underdosage is approximately 5,5 %.

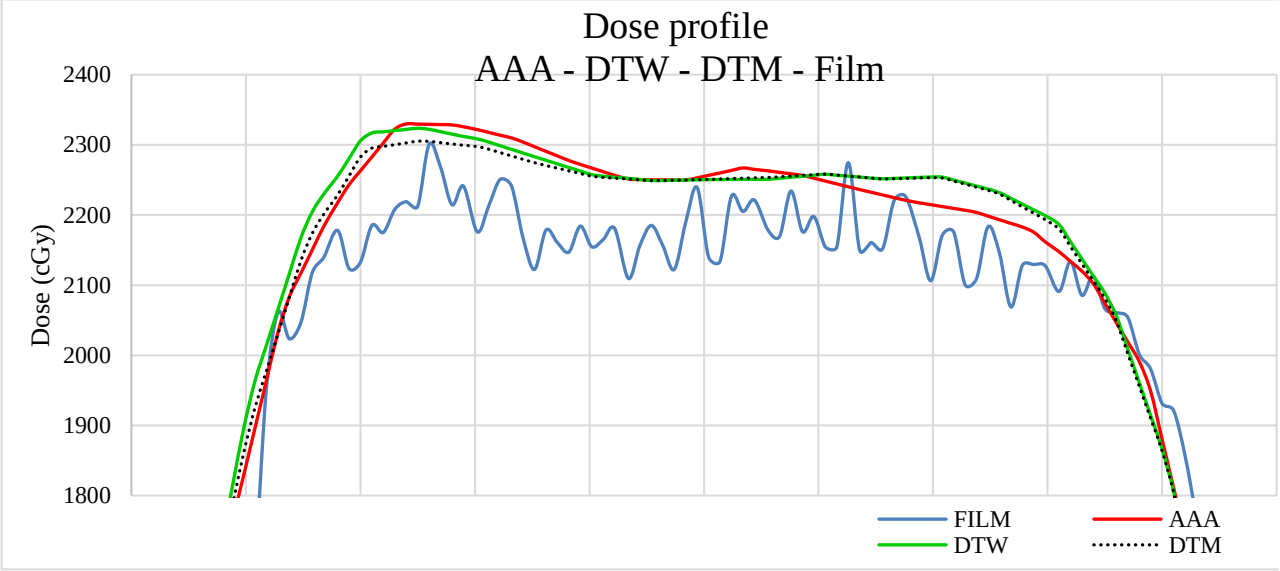

Figure 26: Comparison of the dose profiles for each calculated algorithm (AAA, AXB_W and AXB_M) and the film dose in the center of the tumor.

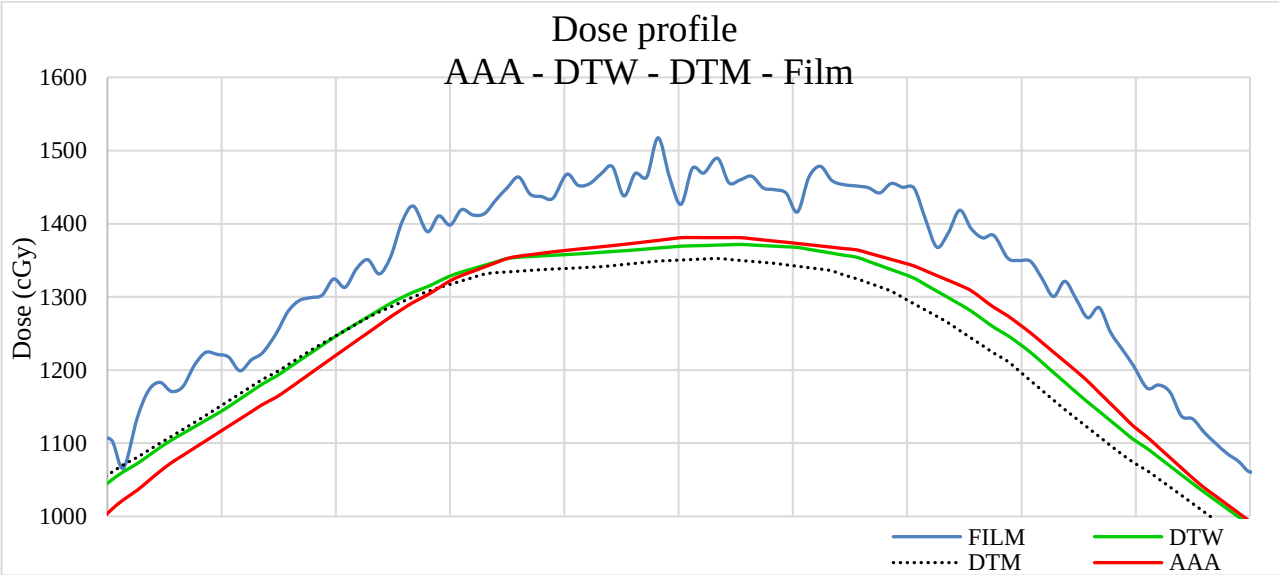

Figure 27: Comparison of the dose profiles for each calculated algorithm (AAA, AXB_W and AXB_M) and the film dose above the tumor.

Figure 28, Figure 29 and Figure 30 depict the gamma maps for comparing the film dose in the center of the tumor with the recalculated dose of the TPS for respectively AAA, AXB_W and AXB_M.
The gamma analysis of the AAA dose map and the film shows small dose differences over the whole 2D dose distribution, varying from 0,00 % to 0,90 %, for Figure 28 and Figure 29. When reviewing the gamma map of the film dose and AXB_M dose map in Figure 30, a dose difference of up to 1,63 % is noticeable, although this is very limited.

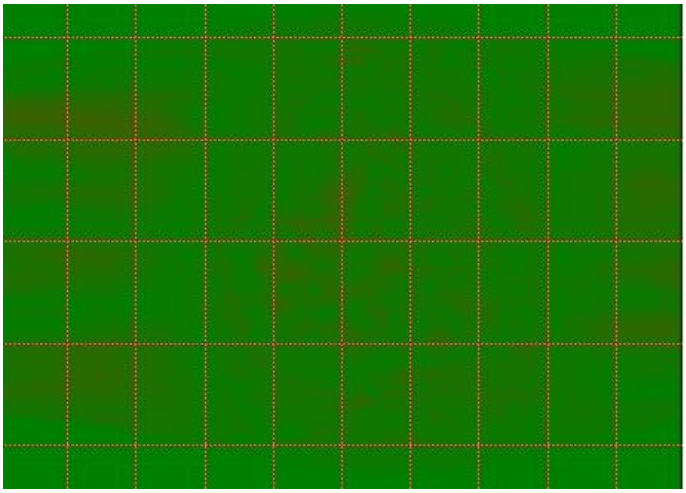

Figure 28: Gamma analysis of film dose and AAA dose map in the center of the tumor.

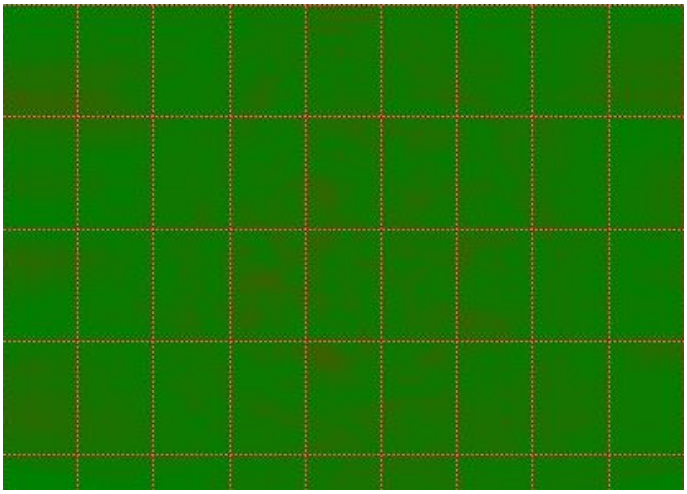

Figure 29: Gamma analysis of film dose and AXB_W dose map in the center of the tumor.

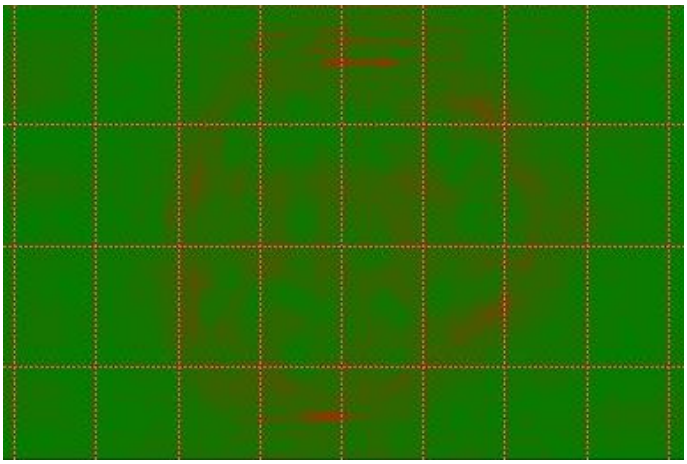

Figure 30: Gamma analysis of film dose and AXB_M dose map in the center of the tumor.

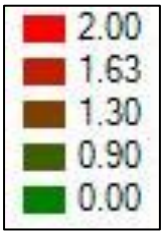

Figure 31, Figure 32 and Figure 33 display the gamma analysis results for comparing the film dose above the tumor with the recalculated dose of the TPS for respectively AAA, AXB_W and AXB_M. The dose differences in Figure 31 are limited to 1,30 %, for the gamma map of film dose and AXB_W, dose differences up to 1,63 % are noticeable. A dose difference of up to 2 % can be found in the gamma map of film dose and AXB_M.

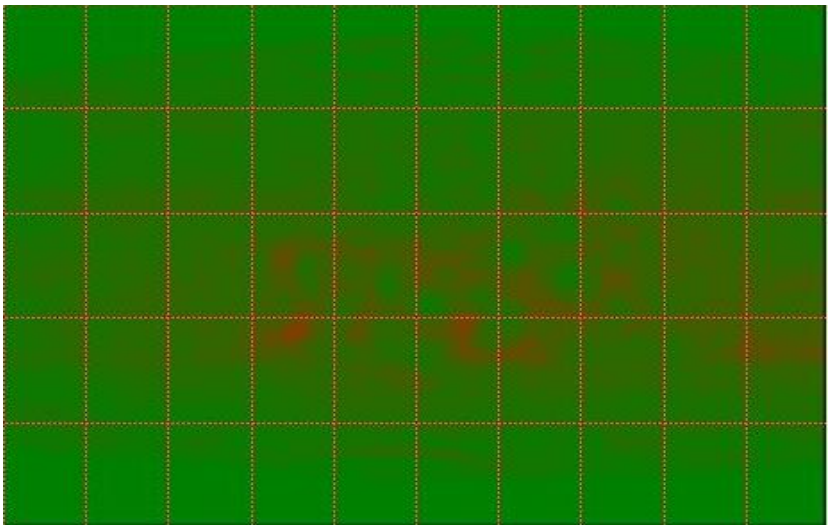

Figure 31: Gamma analysis of film dose and AAA dose map above the tumor.

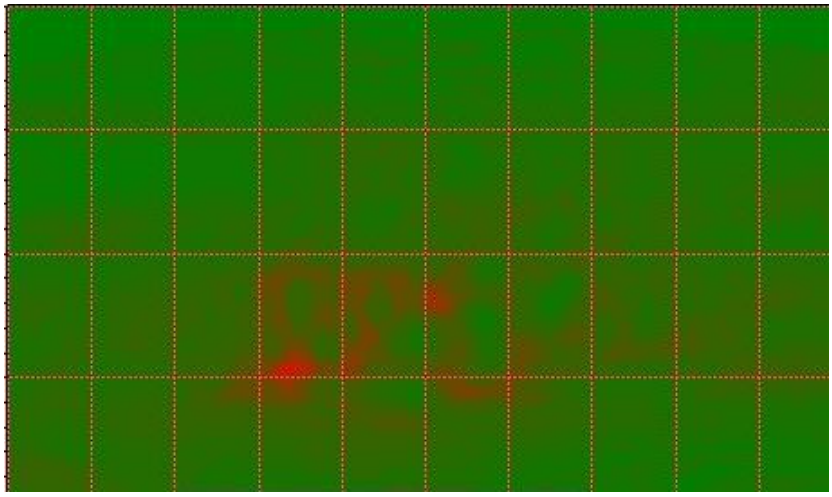

Figure 32: Gamma analysis of film dose and AXB_W dose map above the tumor.

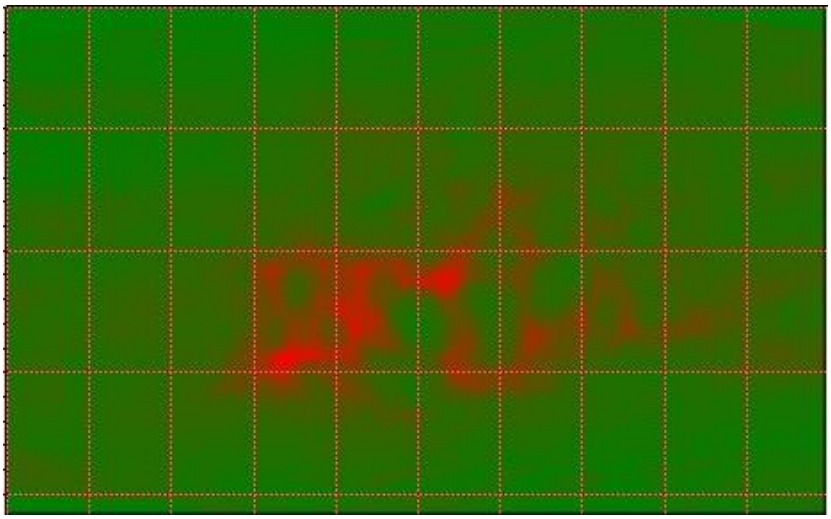

Figure 33: Gamma analysis of film dose and AXB_M dose map above the tumor.

4.2.7. Test 3: 2 arcs

Figure 34 displays the horizontal dose profiles for each calculated dose plan (AAA, AXB_W and AXB_M) compared with the dose of the film, all in the center of the tumor. All profiles are in accordance with the film dose. No significant dose differences between AAA, AXB_W and AXB_M can be noticed, although a 3,0 % dose difference in the right area of the graph is noticeable.
Figure 35 depicts the horizontal dose profiles for each calculated dose plan (AAA, AXB_W and AXB_M) compared with the dose of the film, all at the same height above the tumor, and more specific, at the lung-soft tissue transition. No significant dose differences between the dose maps of AAA, AXB_W and AXB_M can be noticed, but the difference between the film and the calculated dose is apparent and very high.

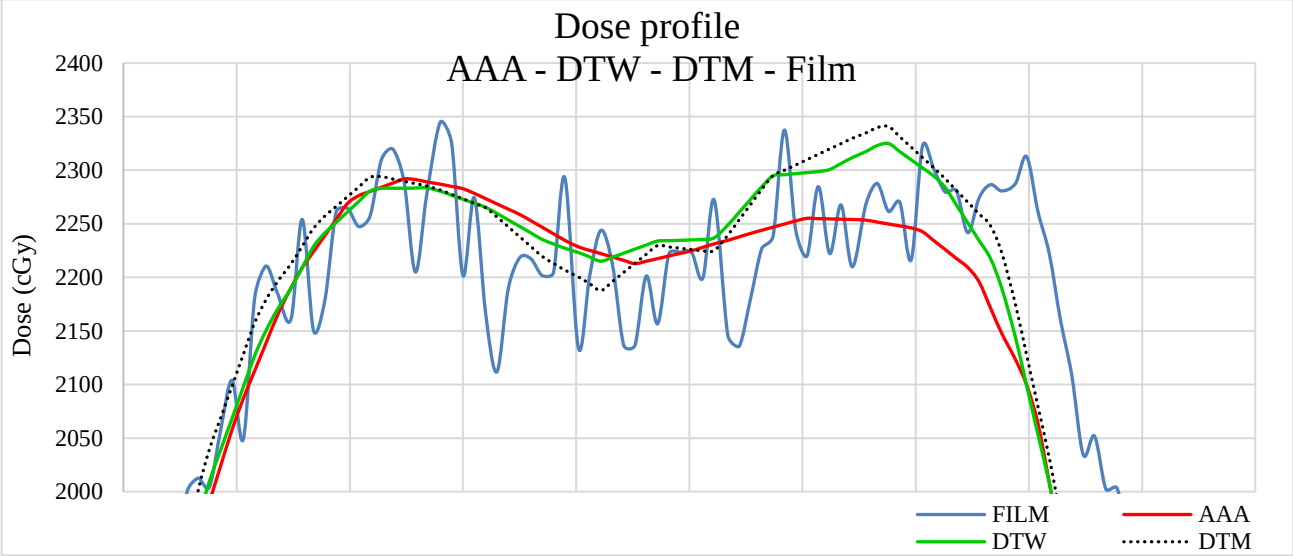

Figure 34: Comparison of the dose profiles for each calculated algorithm (AAA, AXB_W and AXB_M) and the film dose in the center of the tumor.

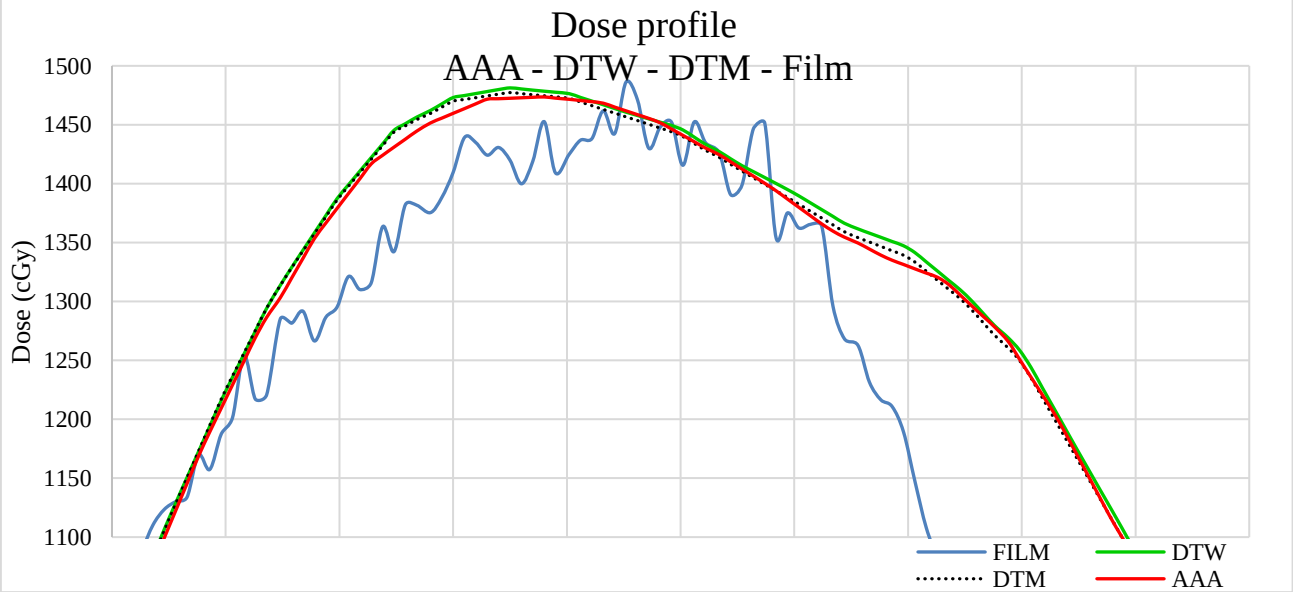

Figure 35: Comparison of the dose profiles for each calculated algorithm (AAA, AXB_W and AXB_M) and the film dose above the tumor.

Figure 36, Figure 37 and Figure 38 display the gamma analysis results for comparing the film dose in the center of the tumor with the recalculated dose of the TPS for respectively AAA, AXB_W and AXB_M.
The three gamma maps, depicted above, show only small dose differences over the whole 2D dose distribution, varying from 0,00 % to 1,30 %, based on the legenda provided by the Film QA Pro Software.

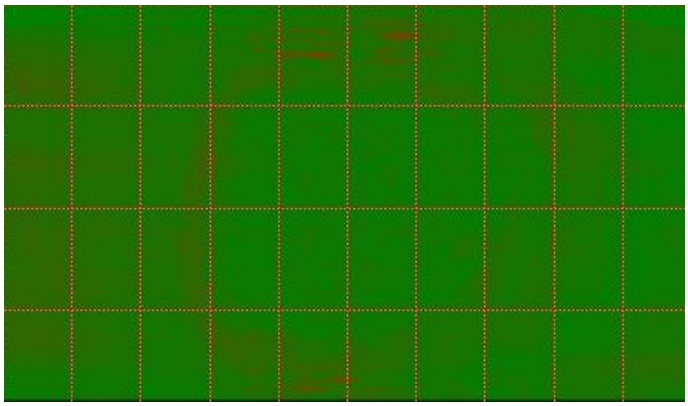

Figure 36: Gamma analysis of film dose and AAA dose map in center of the tumor.

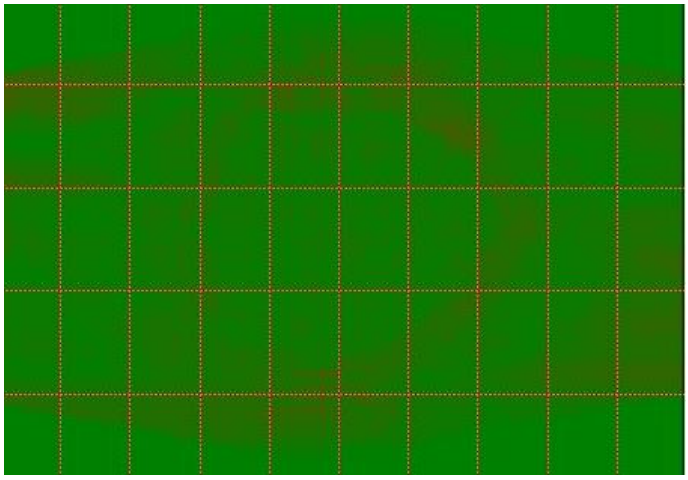

Figure 37: Gamma analysis of film dose and AXB_W dose map in center of the tumor.

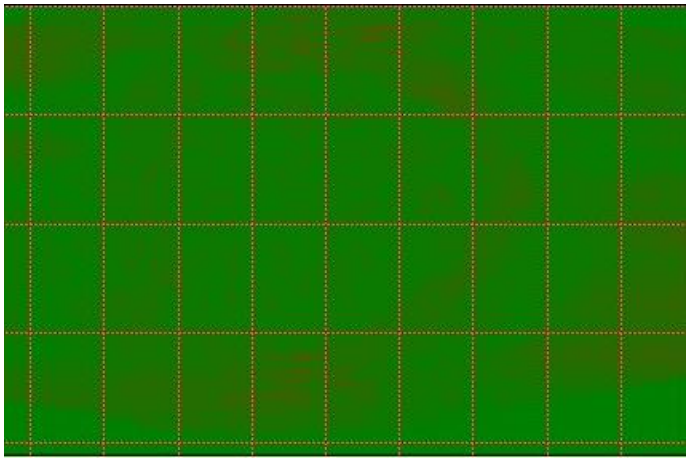

Figure 38: Gamma analysis of film dose and AXB_M dose map in center of the tumor.

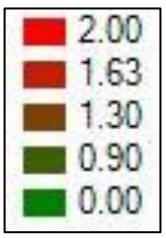

Figure 39, Figure 40 and Figure 41 display the gamma analysis results for comparing the film dose above the tumor with the recalculated dose of the TPS for respectively AAA, AXB_W and AXB_M. The dose differences of the three gamma maps mentioned earlier are significantly larger than the maximum difference in the Film QA Pro legenda. When comparing the TPS and the film dose, the dose differences of Figure 35 is consistent with the dose differences of the gamma maps of Figure 39, Figure 40 and Figure 41.

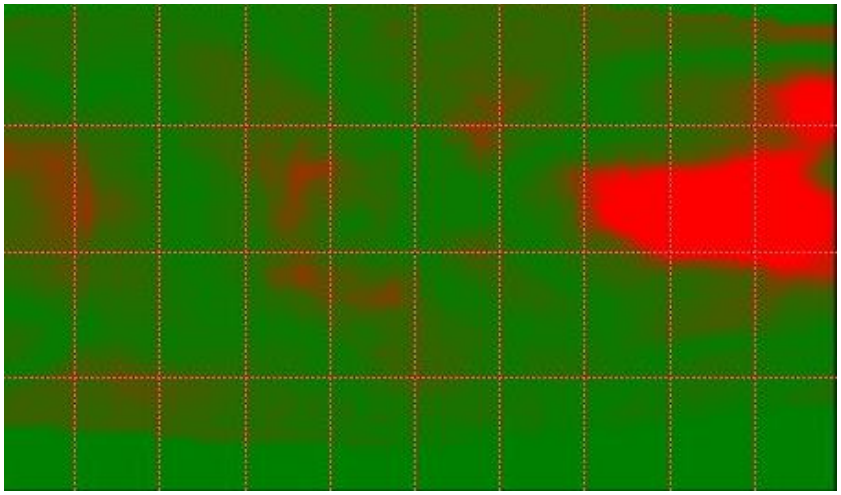

Figure 39: Gamma analysis of film dose and AAA dose map above the tumor.

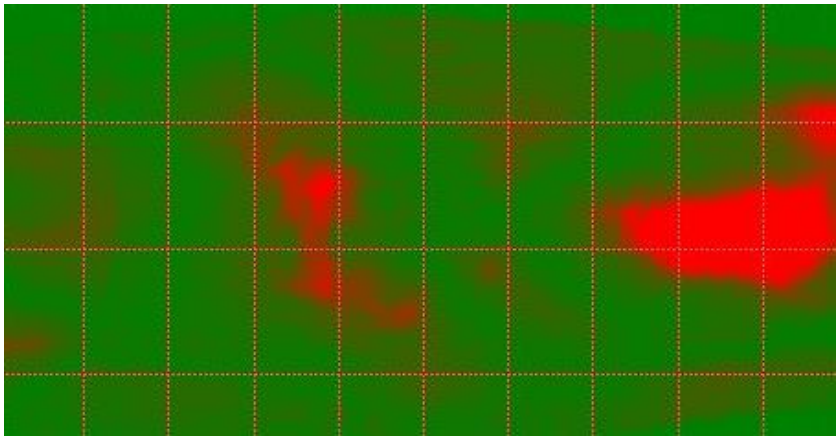

Figure 40: Gamma analysis of film dose and AXB_W dose map above the tumor.

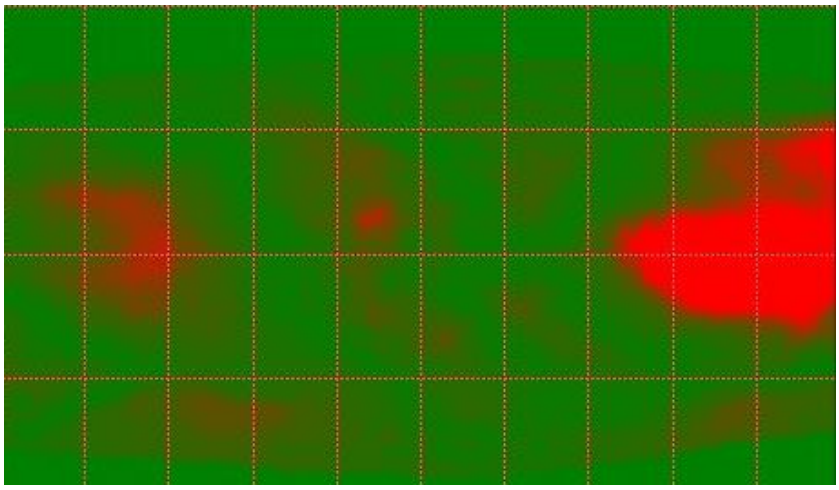

Figure 41: Gamma analysis of film dose and AXB_M dose map above the tumor.

4.3. Comparison dose results recalculations and phantom tests

Figure 42 displays the absolute percentage differences of Acuros in comparison to AAA, not only for the 60 recalculated SBRT plans, but compared to the dose differences of the two last phantom tests. Although, one cannot possibly compare the statistical uncertainty of 60 SBRT plans against only two plans, this graph gives an indication of the dose deviation occurred for an individual plan when recalculated with Acuros. Although, AAA underestimates the dose in the PTV by mean value of 5,6 %, the dose deviations are highly dependent on the nearby tissue composition. This was clearly established by the results of the phantom specific tests.

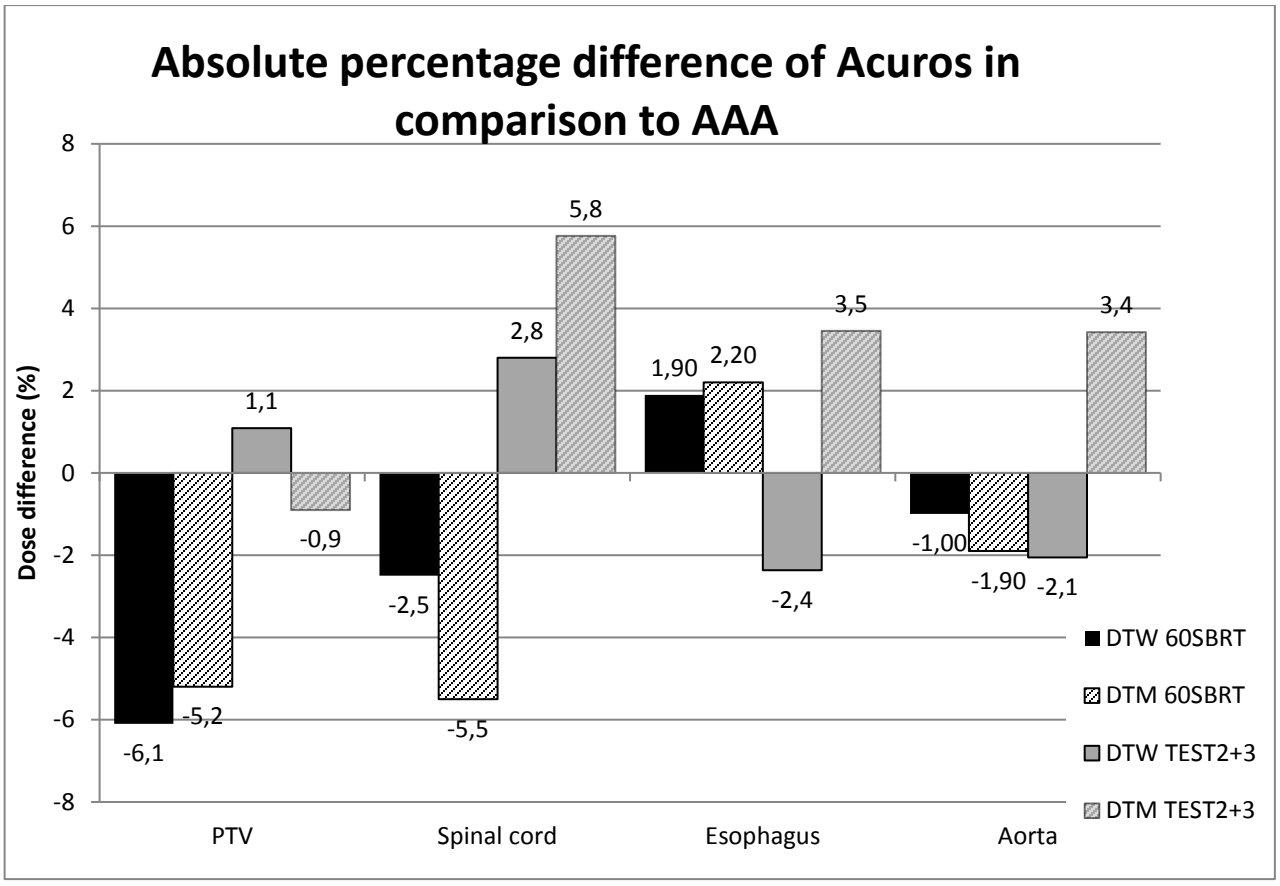

Figure 42: Absolute percentage difference of Acuros in comparison to AAA. The results of the 60 recalculated SBRT plans (black) are compared to the dose results of phantom test 2 and 3 (grey).

5. Discussion

5.1. Recalculation of patient plans

By recalculating these patient plans, a statistical estimation can be found on the overall dose difference for delineated structures for the calculation algorithms. the dose difference in the whole delineated structure is averaged out and reduced to one number. However, the delivered dose should not be assessed by a 1D comparison. Since the delivered dose within every delineated structure, and especially the PTV or structure very near the PTV, can have a broad spectrum, a more detailed dose comparison in 2D or 3D needs to be established. A 2D dose comparison can compare the dose of the different algorithms to the actual delivered dose, in a more detailed way.

5.2. Patient specific phantom study

5.2.1. Phantom test 1: 3 static fields

Firstly, this plan was used to test the set up. All dose differences remained within the uncertainty limits caused by the film and the alanine. The dose profiles show a good agreement, not only the profiles of the irradiated film and calculated TPS in the center of the tumor, but the profiles above the tumor as well. These results are confirmed by the gamma maps. The gamma analysis of the AAA dose map and the film above the tumor shows no dose difference over the whole 2D dose distribution that was registered. Since the film is irradiated with the plan calculated for AAA, this result was expected.
The criteria of dose difference <3 % and distance-to-agreement <2mm were applied for all gamma maps. For this 3 %/2 mm criteria, the passing rate is 99 % at the green channel for the gamma maps at the center of the tumor. A passing rate of 99 % could not be reached for all gamma maps above the tumor, a minimum of 88 % was reached for all gamma maps above the tumor. Also, the irradiation plan with three static fields is a simplified SBRT treatment plan. Furthermore, only one OAR (esophagus) was delineated in this plan, which didn't cause any challenges for the calculation engine. There are also no significant dose differences within the different calculation algorithms (AAA, AXB_W and AXB_M).

5.2.2. Phantom test 2: 2 arcs

The dose profiles for the calculated algorithms by the TPS (AAA, AXB_W and AXB_M) are all very similar. However, when the dose profile of the film dose is compared to the dose profiles calculated by the TPS, firstly an underdosage of approximately 1,73 % for the film dose is noticeable in the center of the tumor, and secondly, above the tumor, the film dose shows an overdosage of approximately 5,50 %, over the whole length of the film. The TPS for AXB_M shows the largest difference compared to the film.
The gamma maps that compared the dose in the center of the tumor, all verify the agreement in dose that is also present on the dose profiles in Figure 26. The overdosage of the TPS resembles a dose difference of 1,7%. This is within the uncertainty limits of the film dose itself.
The gamma maps as a result of the film and TPS dose above the tumor, show less dose differences than the dose profiles in Figure 27. The gamma map that compared the film dose to the calculated dose for AXB_M also shows the least dose agreement with the film dose, as this was the case in Figure 27.

5.2.3. Phantom test 3: 2 arcs

When using the OneScan method for rescaling the film dose. The highest dose of the two reference films (0 Gy and 16 Gy) should have received a dose that is in the region of the maximum dose of the application film or about 20 % higher than the dose received by the application film [26]. With test 3, this was not the case, hence the dose difference between TPS and film when using the OneScan method, visualized in Figure 17.
The gamma maps of test 3 show minimal dose differences in the center of the tumor. However, significant dose differences, larger than 2 % can be seen very clearly on the gamma maps of the film that was positioned above the tumor.

5.2.4. General

In general, all tests show only small and insignificant dose differences for the films placed and the algorithms calculated in the center of the tumor.
During the experiments, an inconvenience with the hydrogel was noticed, as can be seen in Figure 43 below. Hydrogel as a tumor equivalent material has proven its advantages and disadvantages in this study. First of all, hydrogel is inexpensive and widely available. It is a flexible, odorless, biologically nontoxic material, and can be adjusted to the density of a tumor. Secondly, hydrogels tend to lose water and undergo deformation, which is not suitable for long-time use. Furthermore, as the hydrogel retracts after being poured in the 3D printed boxes, this resulted in a horizontal air gap in the center plane when assembling the phantom. Thus, the tumor consists of not only hydrogel, but also air in the middle plane. Yet, the influence of the air on the dose remained minimal when comparing the calculated dose of the delineated alanine to the read out of the EPR spectrometer to the TPS. A viable explanation could be that the air gap on CT appears larger due to the partial volume effect (PVE) than it actually is. The relative dose difference of the dose on TPS/alanine read out is 3,0 % as displayed in Table 6.

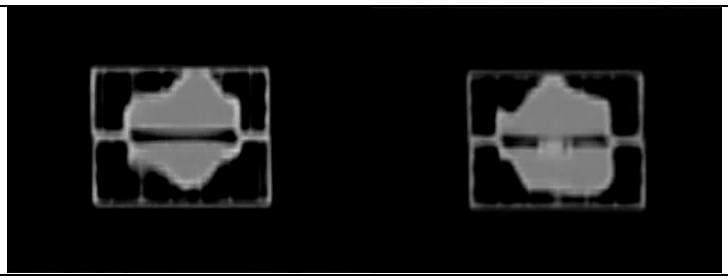

Figure 43: Axial CT-slice through the hydrogel tumor, used for phantom test 3.

Despite the air gap in the tumor center, dose differences in between the different algorithms (AAA, AXB_W and AXB_M) are small and not significant. Since this is at the center of the tumor, and there are no large inhomogeneities, this result was expected.
However, the dose differences of the film and the TPS are much larger above the tumor. All calculation algorithms show larger deviations with the actual delivered dose to the film, as can be seen on the dose profiles of Figure 35 and the associated gamma maps in Figure 39, Figure 40 and Figure 41. Firstly, the dose difference is larger since this is an interface. Dose calculation at the substance boundary of two tissues with a large density gradient is the most difficult case for the TPS. Despite the inhomogeneities, a better resemblance for the dose calculation of Acuros, and especially for AXB_M was expected. Secondly, this zone is considered a low dose region, which means the dose will be spread out more.

If the results of the recalculations of the patient plans are compared to the three phantom tests, we can conclude that the mean underdosage of 6,1 % (AXB_W) and 5,2 % (AXB_M) from the SBRT plan recalculations was not observed in the dose profiles of the phantom tests

6. Conclusion

By recalculating SBRT plans and comparing the dose for AAA, AXB_W and AXB_M, the dose differences for the PTV and other delineated organs gave an indication of how the dose changes, depending on the algorithm.
From this point of view, a dose verification phantom was developed, not only for dose verification but also for dose evaluation of the algorithms.

Firstly, performing personalized dose verification using the Virtual Water IMRT Dose Verification Phantom presented a successful outcome in this master's thesis. The dose in the tumor can be verified using the TPS, the alanine and the radiochromic film. The dose of the OAR was not verified with film or alanine in this Master's thesis. However, in the current set up, the dose for OAR can be verified at height of the radiochromic film and only for OAR near the tumor (depending on the film size). More OAR or tissues can be evaluated when adding more films to the phantom. The dose of the OAR was evaluated by the TPS.
Additionally, we have come across some difficulties concerning the tumor equivalent material, in terms of undeformability and long-term use. Further research must be done to develop a non-organic tumor equivalent material.

Besides, working with a phantom, radiochromic films, and alanine, in the context of dose verification and evaluation has proven to be a challenging practice. Evaluating dose differences that are affected by several uncertainties, such as inherent properties of the film, the calibration method and the phantom set up, demonstrates not only the amount of caution that must be taken when developing a dose verification system but also that one must account for all possible parameters that may have affected the final outcome.
Finally, the dose differences in between AAA and Acuros (AXB_W and AXB_M) as a result of the plan recalculations cannot be confirm or denied with the three specific phantom tests. Yet, we can verify that the largest dose differences are at the substance boundaries.

On short term, there is no standard protocol to evaluate the dose differences between AAA and Acuros. The phantom tests have proven that several uncertainties make it hard to evaluate the dose difference as well as the fact that the dose differences can vary a lot from plan to plan.

Further long-term research can and needs to be done to evaluate the clinical progress and implications of Acuros dose calculation. However, a clear answer will quite certainly not be found. Since the dose differences are too small and other external factors should be considered, it will be very challenging to do research on the impact of this single effect. If an impact is present, it will take years to become noticeable and exceptionally hard to tell if the change to the Acuros algorithm has caused this.

References

[1] C. Eduardo *et al.*, "Stereotactic body radiotherapy in lung cancer: an update," vol. 41, no. May, pp. 376–387, 2015.

[2] K. O. Centre, "Radical radiotherapy for stage I / II non-small cell lung cancer in patients not sufficiently fit for or declining surgery (medically inoperable): a systematic review," pp. 628–638, 2001.

[3] N. Ahmed, S. Hasan, L. Schumacher, A. Colonias, and R. E. Wegner, "Stereotactic body radiotherapy for central lung tumors: Finding the balance between safety and efficacy in the 'no fly' zone," vol. 9, pp. 1211–1214, 2018.

[4] A. Loblaw, S. Liu, and P. Cheung, "Stereotactic ablative body radiotherapy in patients with prostate cancer," vol. 2017, no. 3, pp. 330–340, 2018.

[5] M. C. Aznar, S. Warren, M. Hoogeman, and M. Josipovic, "The impact of technology on the changing practice of lung SBRT," *Phys. Medica*, vol. 47, no. November 2017, pp. 129–138, 2018.

[6] E. M. Dunne, I. M. Fraser, and M. Liu, "Stereotactic body radiation therapy for lung, spine and oligometastatic disease: current evidence and future directions," vol. 6, no. 4, 2018.

[7] K. N. Franks, P. Jain, and M. P. Snee, "Stereotactic Ablative Body Radiotherapy for Lung Cancer Statement of Search Strategies Used and Basic Principals of Lung Stereotactic Ablative Radiotherapy," *Clin. Oncol.*, vol. 27, no. 5, pp. 280–289, 2015.

[8] L. Stalpers, "Radiobiologie : 30 jaar lineair-kwadratisch model," vol. 156, no. 30, pp. 4–10, 2012.

[9] C. W. Song, M. S. Kim, L. C. Cho, K. Dusenbery, and P. W. Sperduto, "Radiobiological basis of SBRT and SRS," *Int. J. Clin. Oncol.*, vol. 19, no. 4, pp. 570–578, 2014.

[10] S. Rehman, M. C. Roach, D. Bradley, and Θ. C. Robinson, "Lung Stereotactic Body Radiation Therapy," no. October, pp. 361–365, 2015.

[11] P. Baumann *et al.*, "Factors important for efficacy of stereotactic body radiotherapy of medically inoperable stage I lung cancer. A retrospective analysis of patients treated in the Nordic countries," 2009.

[12] J. Zeng, C. Baik, S. Bhatia, N. Mayr, and R. Rengan, "Combination of stereotactic ablative body radiation with targeted therapies," *Lancet Oncol.*, vol. 15, no. 10, pp. e426–e434, 2014.

[13] M. D'Andrea *et al.*, "Radiobiological Optimization in Lung Stereotactic Body Radiation Therapy: Are We Ready to Apply Radiobiological Models?," *Front. Oncol.*, vol. 7, no. January, 2018.

[14] L. Dhamers, J. Withouck, K. Bamps, K. Tournel, and B. Reniers, "Implications with the implementation of Acuros: a comparison between AAA and Acuros on dose calculations," Hasselt, 2018.

[15] American Association of Physicists in Medicine, "The use and QA of Biologically Related Models for Treatment Planning Report of AAPM Task Group 166," 2012.

[16] S.-Y. Park, J. M. Park, C. H. Choi, M. Chun, and J. Kim, "Dosimetric Validation of the Acuros XB Advanced Dose Calculation Algorithm for Volumetric Modulated Arc Therapy Plans," *Prog. Med. Phys.*, vol. 27, no. 4, p. 180, 2016.

[17] J. V Siebers, P. Keall, A. E. Nahum, and M. R, "Converting absorbed dose to medium to absorbed dose to water for Monte Carlo based photon beam dose calculations," *Phys. Med. Biol.*, vol. 45, pp. 983–995, 2000.

[18] A. Fogliata, G. Nicolini, A. Clivio, E. Vanetti, and L. Cozzi, "Dosimetric evaluation of Acuros XB Advanced Dose Calculation algorithm in heterogeneous media," *Radiat. Oncol.*, vol. 6, no. 1, p. 82, 2011.

[19] T. Knoos and B. Mcclean, "Dose calculation algorithms in algorithms in 3DCRT and IMRT," in *Medical Physics*, 2008, vol. 35, no. 6, p. 2930.

[20] J. Sievinen, W. Ulmer, and W. Kaissl, *AAA Photon Dose Calculation Model in Eclipse ™*. .

[21] N. Reynaert, F. Crop, E. Sterpin, I. Kawrakow, and H. Palmans, "On the conversion of dose to bone to dose to water in radiotherapy treatment planning systems," *Phys. Imaging Radiat. Oncol.*, vol. 5, no. December 2017, pp. 26–30, 2018.

[22] G. Reggiori *et al.*, "Can volumetric modulated arc therapy with flattening filter free beams play a role in stereotactic body radiotherapy for liver lesions? A volume-based analysis."

[23] V. C. Borca *et al.*, "Dosimetric characterization and use of GAFCHROMIC EBT3 film for IMRT dose verification," *J. Appl. Clin. Med. Phys.*, vol. 14, no. 2, pp. 158–171, 2013.

[24] O. L. Dancewicz, S. R. Sylvander, T. S. Markwell, S. B. Crowe, and J. V Trapp, "Radiological properties of 3D printed materials in kilovoltage and megavoltage photon beams," *Phys. Medica*, vol. 38, pp. 111–118, 2017.
[25] S. Devic, "Radiochromic film dosimetry: Past, present, and future," *Phys. Medica*, vol. 27, no. 3, pp. 122–134, 2011.
[26] D. Lewis, A. Micke, and X. Yu, "An efficient protocol for radiochromic film dosimetry combining calibration and measurement in a single scan," vol. 39, no. 10, pp. 6339–6350, 2012.
[27] A. Micke, D. F. Lewis, and X. Yu, "Multichannel film dosimetry with nonuniformity correction," vol. 07470, no. August 2010, pp. 2523–2534, 2011.
[28] J. Sorriaux *et al.*, "Evaluation of Gafchromic EBT3 films: characteristics in therapy photon, electron and proton beams," *Phys. Medica*, pp. 1–10, 2012.
[29] S. Khachonkham *et al.*, "Characteristic of EBT-XD and EBT3 radiochromic film dosimetry for photon and proton beams," *Phys. Med. Biol.*, vol. 63, no. 6, 2018.
[30] A. Niroomand-Rad *et al.*, "Radiochromic Film Dosimetry: Recommendations of AAPM Radiation Therapy Committee Task Group No. 55," vol. 25, no. 63, 1998.
[31] F. Girard, H. Bouchard, and F. Lacroix, "Reference dosimetry using radiochromic film."
[32] E. Y. L. Marroquin, J. A. H. González, M. A. C. López, J. E. V. Barajas, and O. A. García-garduño, "Evaluation of the uncertainty in an EBT3 film dosimetry system utilizing net optical density," vol. 17, no. 5, pp. 466–481, 2016.
[33] M. Mathot, S. Sobczak, and M. Hoornaert, "Gafchromic film dosimetry: Four years experience using FilmQA Pro software and Epson flatbed scanners," *Phys. Medica*, vol. 30, no. 8, pp. 871–877, 2014.
[34] A. Micke and X. Yu, "Multi-Channel Film Dosimetry & Gamma Map Analysis," 2014, no. May.
[35] B. H. Østerås, E. O. Hole, and D. R. Olsen, "EPR dosimetry of radiotherapy photon beams in inhomogeneous media using alanine films," *Phys. Med. Biol.*, 2006.
[36] O. Baffa and A. Kinoshita, "Clinical applications of alanine/electron spin resonance dosimetry," pp. 233–240, 2014.
[37] M. A. Morsy, "Simple EPR/Alanine Dosimeter for Medical Application," vol. 2012, no. December, pp. 120–125, 2012.
[38] A. M. Al-Karmi, A. A. H. Ayaz, M. S. Al-Enezi, W. Abdel-Rahman, and N. Dwaikat, "Verification of the pure alanine in PMMA tube dosimeter applicability for dosimetry of radiotherapy photon beams: a feasibility study," *Australas. Phys. Eng. Sci. Med.*, vol. 38, no. 3, pp. 425–434, 2015.
[39] B. Schaeken *et al.*, "Implementation of alanine EPR as transfer dosimetry system in a radiotherapy audit programme in Belgium," *Radiother. Oncol.*, vol. 99, no. 1, pp. 94–96, 2011.
[40] V. Nagy, S. V Sholom, V. V Chumak, and M. F. Desrosiers, "Uncertainties in alanine dosimetry in the therapeutic dose range," vol. 56, pp. 917–929, 2002.
[41] Standard Imaging, "IMRT dose verification phantom specifications."
[42] G. Distefano *et al.*, "A national dosimetry audit for stereotactic ablative radiotherapy in lung," *Radiother. Oncol.*, vol. 122, no. 3, pp. 406–410, 2017.
[43] J. M. C. Ye, J. P. Chang, Z. P. Li, A. G. M. Ms. Wernicke, and P. M. Dattatreyudu, Nori MD Bhupesh, "(P097) Tumor Density, Size, and Histology in the Outcome of Stereotactic Body Radiation Therapy for Early-Stage Non–Small-Cell Lung Cancer: A Single-Institution Experience," *CancerNetwork, Oncol.*, vol. 29, 2015.
[44] M. Anton, "Development of a secondary standard for the absorbed dose to water based on the alanine EPR dosimetry system," vol. 62, pp. 779–795, 2005.
[45] H. Miura *et al.*, "Gafchromic EBT-XD film: Dosimetry characterization in high-dose, volumetric-modulated arc therapy," *J. Appl. Clin. Med. Phys.*, vol. 17, no. 6, pp. 312–322, 2016.